Coaction of intercellular adhesion and cortical tension specifies tissue surface tension

M. Lisa Manning[a], Ramsey A. Foty[b], Malcolm S. Steinberg[c], and Eva-Maria Schoetz[d,1]

[a]Princeton Center for Theoretical Science, Princeton University, Princeton, NJ 08544; [b]University of Medicine and Dentistry of New Jersey-Robert Wood Johnson Medical School, Piscataway, NJ 08854; [c]Department of Molecular Biology, Princeton University, Princeton, NJ 08544; and [d]Lewis-Sigler Institute for Integrative Genomics, Princeton University, Princeton, NJ 08544

Edited* by Barry H. Honig, Columbia University/Howard Hughes Medical Institute, New York, NY, and approved June 7, 2010 (received for review March 20, 2010)

In the course of animal morphogenesis, large-scale cell movements occur, which involve the rearrangement, mutual spreading, and compartmentalization of cell populations in specific configurations. Morphogenetic cell rearrangements such as cell sorting and mutual tissue spreading have been compared with the behaviors of immiscible liquids, which they closely resemble. Based on this similarity, it has been proposed that tissues behave as liquids and possess a characteristic surface tension, which arises as a collective, macroscopic property of groups of mobile, cohering cells. But how are tissue surface tensions generated? Different theories have been proposed to explain how mesoscopic cell properties such as cell–cell adhesion and contractility of cell interfaces may underlie tissue surface tensions. Although recent work suggests that both may be contributors, an explicit model for the dependence of tissue surface tension on these mesoscopic parameters has been missing. Here we show explicitly that the ratio of adhesion to cortical tension determines tissue surface tension. Our minimal model successfully explains the available experimental data and makes predictions, based on the feedback between mechanical energy and geometry, about the shapes of aggregate surface cells, which we verify experimentally. This model indicates that there is a crossover from adhesion dominated to cortical-tension dominated behavior as a function of the ratio between these two quantities.

differential adhesion hypothesis | differential interfacial tension hypothesis | mathematical modeling | cell aggregate geometry | self-assembly

It is well established that many tissues behave like liquids on long timescales. Cell tracking in vivo and in vitro highlights (*i*) large-scale flows, (*ii*) exchange of nearest neighbors in a cellular aggregate, and (*iii*) rounding-up and fusion of aggregates (1). Macroscopic rheological properties such as surface tension can be measured using a tissue surface tensiometer (TST) (1–8) or micropipette aspiration (9), and surface tension can be used to explain tissue self-organization in embryogenesis (8, 10–12) or cancer (13, 14). In particular, cell sorting and tissue spreading can be explained in terms of tissue surface tensions that differ among cell types (1, 3–5, 8, 15, 16).

A full understanding of tissue surface tension as a driving force for biological processes is important, and knowledge of its cellular origins would allow us to intelligently design drugs and treatments to alter tissue organization. Two opposing theories about the mesoscopic origin of tissue surface tension have coexisted over the last 30 years. One, the differential adhesion hypothesis (DAH), postulates that in analogy to ordinary fluids, tissue surface tension is proportional to the intensity of the adhesive energy between the constituent cells, which are treated as point objects. The DAH has proven successful in a variety of studies with cell lines (2–5, 15) , malignant (13, 14) and embryonic tissues (1, 5, 8, 16) and is widely accepted (12, 17). A recent study by Foty and Steinberg (18) experimentally verified a linear relationship between adhesion molecule expression levels and tissue surface tension.

However, recent experiments using atomic force microscopy (AFM) (19) and TST (see data in this study) indicate a dependence of the surface tension on actin-myosin activity in the cell, interpreted as supporting an alternative theory in which cortical tension in individual cells is thought to be the determining factor. The differential interfacial tension hypothesis (DITH) developed by Harris (20), Brodland (21), and Graner (22) relates tissue surface tension to the tension along individual cell interfaces. The DITH theories are appealing because they recognize that individual cells are not point objects; a cell's mechanical energy changes with cell shape and the cortical tension clearly plays a role in this energy balance.

Recent work has emphasized that interfacial tensions arise from a balance of adhesion, cortical tension, and cortical elasticity (17, 19, 23, 24). However, the exact nature of this interplay remains to be elucidated.

In this study, we develop, analytically solve, and experimentally verify a model that specifies an explicit relationship between surface tension and the ratio of adhesion to cortical tension. With this model, we can also explain why the DAH, despite its simplicity, is so successful. Furthermore, we predict regimes where the DAH breaks down and, unlike previous models, show that changes in tissue surface tension must be accompanied by changes in the shapes of surface cells as a function of the ratio between adhesion and cortical tension. In the discussion, we propose future experiments, involving laser ablation and long-time AFM measurement, which could be used to further test the various aspects of our model.

Results

Theoretical Description. We develop a minimal mechanical model based on two experimental systems, zebrafish embryonic tissues and a P-cadherin-transfected L-cell line (LP2). Fig. 1*A* is a confocal section of a zebrafish aggregate, showing that cells in the bulk are roughly polyhedral with sharp corners, an aspect ratio of unity and without obvious polarization. The rate of cell divisions in zebrafish aggregates is low (1) and cells within a single tissue type are approximately the same size (see Fig. 1*A*). Our model therefore enforces a constant volume for individual cells, $V = 1$, where we have normalized all volumes by the average volume for a single cell.

Because our goal is to understand the collective behavior of cell populations, we can focus on coarse-grained mechanical properties of individual cells such as cortical tension and adhesion. As in other cell models (23, 25, 26), we associate an energy with cell–cell

Author contributions: M.L.M. and E.-M.S. designed research; M.L.M., R.A.F., M.S.S., and E.-M.S. performed research; M.L.M., R.A.F., and E.-M.S. analyzed data; and M.L.M., R.A.F., M.S.S., and E.-M.S. wrote the paper.

The authors declare no conflict of interest.

*This Direct Submission article had a prearranged editor.

[1]To whom correspondence should be addressed. E-mail: eschoetz@princeton.edu.

This article contains supporting information online at www.pnas.org/lookup/suppl/doi:10.1073/pnas.1003743107/-/DCSupplemental.

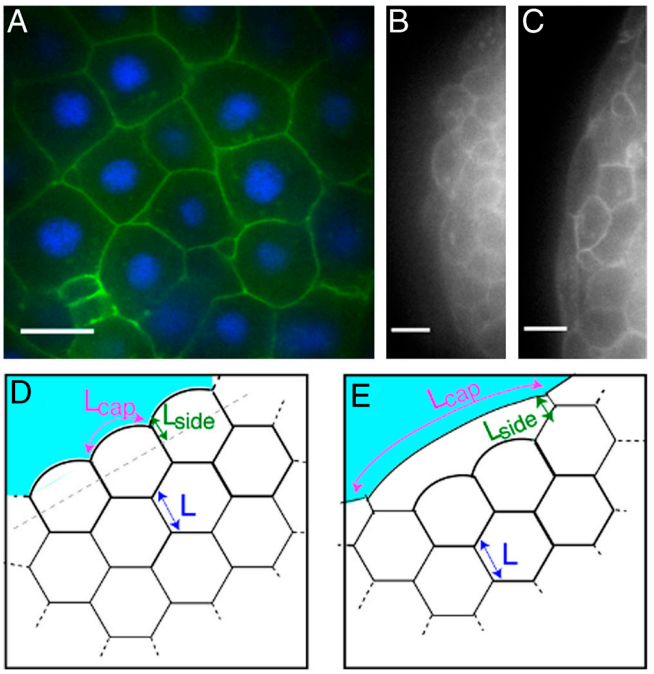

Fig. 1. (*A*–*C*) Confocal sections of zebrafish aggregates. (Scale bar, 10 μm.) (*A*) Ectoderm cells in the bulk are densely packed into roughly polyhedral shapes. Membranes are labeled using Gap43-GFP, nuclei using Hoechst. (*B*) Surface cells in which E-cadherin is down-regulated. Cells have rounded edges and are compact. (*C*) Surface cells of an ectoderm aggregate. Bulk cells are compact, whereas surface cells are stretched. (*D* and *E*) Illustration of ordered packing of cells, where surface cells contact each other over a length L_{side}. (*D*) Cells along the interface with cell–culture medium maintain a compact shape ($n_{stretch} = 1$). (*E*) Illustration of stretched surface cells with $n_{stretch} = 3$. This arrangement satisfies force balance and the constant area constraint.

contacts, where the energy is proportional to the surface area of contact between cells: $W_{ad} = (\Gamma/2)P_C$, where P_C is the surface area (perimeter in 2D) in contact with other cells. In addition, the response of single cells to low-frequency pressures and forces can be characterized by a cortical tension (23, 26, 27): $W_{cort} = \beta P_T$ where P_T is the total surface area of a cell.

Of course, feedbacks between adhesion molecule and cytoskeletal dynamics are abundant, which suggests that the cortical tension along contacting interfaces (β_C) can be different from that along noncontacting interfaces (β_{NC}). Because the cortical-tension energy and adhesive energy both scale linearly with surface area, we can accommodate these feedbacks in a simple way. The term $\beta = \beta_{NC}$ is simply the cortical tension of a cell in the absence of any cell–cell contacts, which is the quantity measured in single-cell pipette aspiration experiments (27). We introduce the *effective adhesion* γ which is the total energetic contribution of contacting surfaces. We define this as the difference between the free energy of the adhesive bonds per unit area (Γ) and local changes to the cortical tension near an interface $2(\beta_C - \beta_{NC})$. Then the coarse-grained mechanical energy for each cell in an aggregate is given by

$$W_{cell} = (\beta - \gamma/2)P_C + \beta P_{NC} \quad |V = 1 \qquad [1]$$

where $P_{NC} = P_T - P_C$ is the surface area of the noncontacting interface. Note that $(\beta - \gamma/2)$ is half the interfacial tension of cell–cell contacts, and β is the interfacial tension of cell–culture medium interfaces. We observe that cells in the interior of aggregates exhibit polyhedral shapes with sharp corners. As discussed in the *SI Text*, this observation means that when $\gamma/\beta < 2$, cortical elasticity must be a small contribution to the energy (at least on the relevant long timescales over which surface tension is a meaningful quantity). Therefore Eq. **1** neglects elastic terms and is valid when $\gamma/\beta < 2$; we discuss the case $\gamma/\beta > 2$ in a later section.

Previous methods for approximating tissue surface tension assumed that individual cells do not change their shapes; in this case, the surface tension is simply the difference between the interfacial tensions of cell–cell and cell–culture medium interfaces (21, 26). However, confocal images of the equatorial plane of spherical zebrafish aggregates (Fig. 1 *B* and *C*) suggest that surface cell shape depends on tissue surface tension, i.e., that there is an interplay between mechanical energy and geometry that must be taken into account. Therefore our strategy will be to find shapes and configurations of cells which locally minimize the mechanical energy and calculate the surface tension of those configurations.

When an aggregate of cells is compressed, the surface area of the aggregate increases, and cells formerly in the bulk are exposed to the surface. Therefore, in exact analogy with fluids, the response of the tissue to changes in surface area is the difference in energy, ΔW, between a cell in the bulk and a cell on the surface, multiplied by the number of cells per unit area (or length in 2D) at the surface. The number of cells per unit area is equal to unity divided by the projected area A_{proj} (or projected length in 2D) of a single cell onto the surface of the aggregate:

$$\sigma = (W_{surf} - W_{bulk})/A_{proj} \qquad [2]$$

In general, this quantity is difficult to calculate for large aggregates because the total energy depends on the exact geometry of each cell in force balance with other cells under the constant volume constraint. However, we have derived an exact solution to this problem for an ordered two-dimensional system.

Analytical and Numerical Results. Fig. 1 *D* and *E* are illustrations of ordered 2D cellular structures with boundaries. Cells in the bulk are hexagonal, all cells have the same fixed area, and individual interfaces must have constant curvature because they are fluid on long timescales and do not support shear stresses. With these constraints, it is possible to parameterize the surface cell shape with only two numbers: L_{side}, which is the length of contact surface cells make with other surface cells, and $n_{stretch}$, which is the number of bulk cells that a surface cell stretches across. Fig. 1*D* illustrates a force-balanced configuration with $n_{stretch} = 1$, and Fig. 1*E* is a configuration with $n_{stretch} = 3$.

The optimal shape can then be explicitly calculated as the values of L_{side} and $n_{stretch}$ that minimize Eq. **1**. Finally, Eq. **2** is used to calculate the surface tension. We find that $n_{stretch} = 1$ always minimizes the energy for $\gamma/\beta < 2$, and the surface tension as a function of γ/β is given by the dashed line in Fig. 2 *A* and *B*. There is a generalization of this calculation to ordered structures in three dimensions, which is detailed in the *SI Text*. The surface tension for 3D-ordered aggregates is given by the dashed line in Fig. 2*C*.

Active processes allow cells to exchange neighbors and explore many possible configurations, so that they are not confined to the global minimum energy configuration. Instead, the collection of cells explores a large number of local minima, and these configurations are disordered, much like the typical configurations of a fluid or a jammed granular material. We use numerical simulations to show that the surface tension for 2D-disordered aggregates is related in a remarkably simple way to that for ordered structures, and make a conjecture about 3D aggregates.

We used the Surface Evolver program developed by Brakke (28) to numerically find the local minimum energy 2D structures for various random initial conditions and values of γ/β (see *Methods*). Fig. 2 *D* and *E* illustrates two minimal structures generated by this procedure: For small values of γ/β, surface cells are rounded (Fig. 2*D*) because they minimize their total perimeter at the expense of cell–cell contacts, whereas, for large values of γ/β, cells are flat (Fig. 2*E*) because they maximize neighbor contacts.

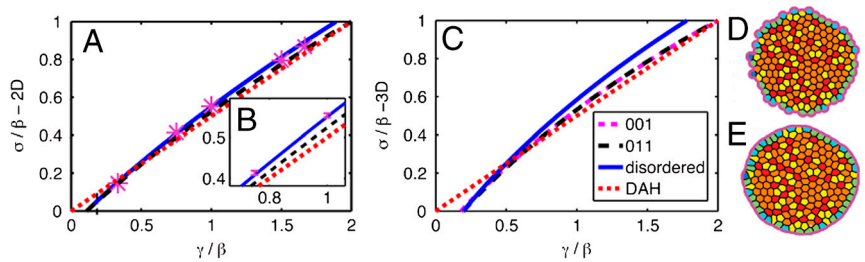

Fig. 2. (*A–C*) Plot of aggregate surface tension in units of β as a function of γ/β. The dashed black line is the analytic calculation for ordered packing σ_{ordered}. The solid blue line is the surface tension for a disordered aggregate. The dotted red line is $\sigma = \gamma/2$, which is equivalent to the DAH. (*A*) Two-dimensional aggregate, $\sigma_{\text{rand}} = 1.05\sigma_{\text{ordered}}$. Magenta points are the average surface tensions of minimum energy aggregates generated numerically. (*B*, *Inset*) Scaled version of 2D data with error bars. (*C*) Three-dimensional aggregate. Blue line is conjectured disordered solution, $\sigma_{\text{disorder}} = 1.10\sigma_{\text{order}}$. (*D* and *E*) Minimum energy cell configurations generated using Surface Evolver at two different values of γ/β. Orange cells have six neighbors. (*D*) Sample aggregate with $\gamma/\beta = 0.33$. (*E*) Same initial conditions as *D* with $\gamma/\beta = 1.667$.

Because the surface tension is a change in energy divided by a projected length, we calculated both of these quantities for individual cells in each numerical simulation. We find that the projected length, which corresponds to the macroscopic perimeter of the entire aggregate, is the only quantity changed by the disorder in the limit of small γ/β. The total area cannot change because the number of cells with fixed area is constant. Because the macroscopic shape of a 2D hexagonal ordered crystal has hexagonal symmetry, whereas the disordered structure is spherically symmetric, this suggests that the macroscopic perimeter should change as the ratio of the perimeter of a hexagon to a circle of the same area: $\sigma_{\text{disorder}} = 1.05\sigma_{\text{order}}$.

This amazingly simple ansatz is tested numerically in Fig. 2 *A* and *B*. The blue line is the analytical expression for σ_{disorder}, whereas each of the magenta stars corresponds to the average surface tension of six numerically minimized aggregates with disordered initial conditions. There is excellent agreement at small values of γ/β, and systematic deviations at large values of γ/β that are easily understood. The geometry places a strict constraint on the macroscopic surface tension when $\gamma = 2\beta$. As γ approaches 2β, the tension along cell–cell interfaces approaches zero and force balance requires that cell-culture medium interface is flat (see *SI Text*). Then the macroscopic surface tension is identically the cortical tension at $\gamma = 2\beta$, and the disordered structures interpolate between the blue line and this value as γ/β increases.

LP2 and Zebrafish Cell Shape Changes. We were able to test the prediction of surface cell shape changes experimentally in LP2 cells by applying actin-depolymerizing drugs [cytochalasin D (CD) and latrunculin A (LA)] to cell aggregates (See *Methods*), determining their surface tension by TST and imaging the aggregates with SEM. Fig. 3 shows three SEM images of cell aggregates from the LP2 cell line. The control aggregate (Fig. 3*A*) has a relatively high surface tension of 3.16 erg/cm^2. The cells on the surface of this aggregate are so flat that one cannot distinguish between them, and our model suggests that the ratio of adhesion to cortical tension is high for this aggregate. Fig. 3 *B* and *C* are aggregates treated with actin-depolymerizing drugs that reduce the cortical tension as well as cell–cell adhesion as the actin anchor of cadherin bonds is weakened. As expected, the macroscopic surface tension is significantly lower. It is important to note that the effect of actin-depolymerizing drugs on tissue surface tension is reversible (see *SI Text*), and that rounded surface cells are viable cells, as confirmed by viability staining and cell sorting experiments (*SI Text*).

Confocal images of zebrafish surface cells such as those in Fig. 1 *B* and *C* indicate that this shape change is more substantial than going from round to flat: Although our model suggests that structures with $n_{\text{stretch}} = 1$ are the minimum energy states, aggregates with high surface tension often have surface cells which stretch over multiple bulk cells as shown in Fig. 1*B*. These stretched surface cells, however, do not express epithelial markers (see *SI Text*) and express the same tissue-type-specific

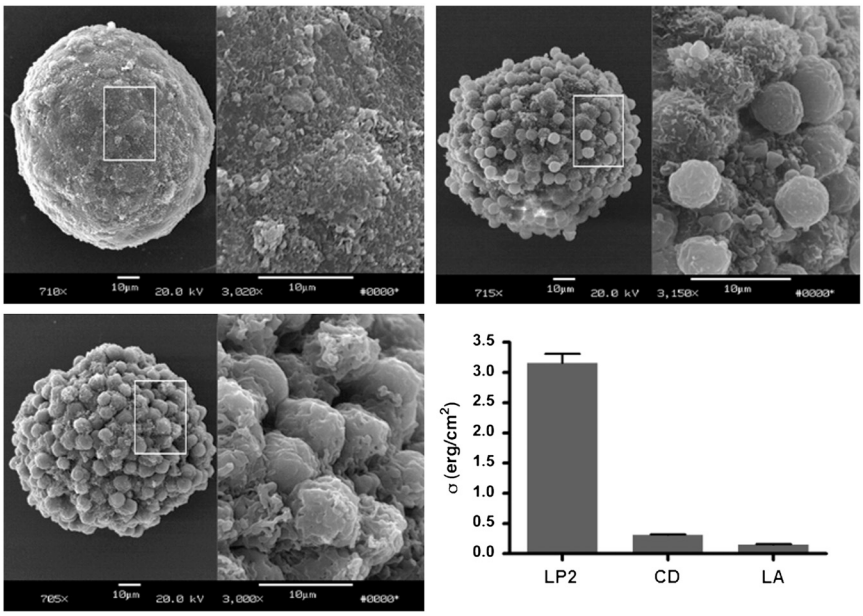

Fig. 3. (*A–C*) SEM images of cell aggregates. (*A*) Control LP cell aggregate. (*B*) Cell aggregate treated with latrunculin A. (*C*) Cell aggregate treated with cytochalasin D. (*D*) Surface tension σ as measured by TST.

markers as bulk cells (1). Furthermore, they are also indistinguishable in their behavior as surface cells become intermixed with bulk cells during aggregate fusion (1) and cells continue to diffuse in and out of the surface layer (see *SI Text*). We now extend our model to account for these stretched cells and investigate the phenomenon quantitatively in experiments.

Modeling Stretched Cell Shapes. When the adhesion is greater than the cortical tension, our mechanical model Eq. **1** predicts that cells will begin to spread out because the line tension is negative, $dW/dP = -\gamma/2 + \beta < 0$, so cells will continue to increase their perimeter without limit. This perimeter growth cannot continue unabated because other mechanical forces will eventually cause the cells to stop expanding.

What additional restoring force is consistent with experimental observations? Adhesion molecule regulation generates a plausible restoring force; the amount of energy a single cell can gain by increasing its perimeter must be limited by the number of cadherins on the cell surface, which is itself regulated. Although we do not know the exact form of this regulation, we can expand its energetic contribution as a Taylor series in the difference between the actual adhesive energy and the adhesive energy of a cell with the preferred number of cadherins. Keeping up to second-order terms, this adds a term αP_C^2 to Eq. **1**, as discussed in the *SI Text*. Another possible restoring force is elasticity generated by a denser cortical network near cell–cell interfaces; this would also add a term proportional to P_C^2 (22, 24). The remaining analysis does not depend on the mechanistic origin of these forces, but simply requires that the first higher-order term is of the form P_C^2:

$$W_{\text{cell}} = (\beta - \gamma/2)P_C + \alpha P_C^2 + \beta P_{\text{NC}} \quad |V = 1 \qquad [3]$$

The lowest energy states corresponding to this energy functional are complicated because the P_c^2 term introduces a length scale that is not necessarily the same as the length scale introduced by the incompressibility constraint. For example, in two dimensions, the smallest perimeter structure is hexagonal, but the preferred perimeter introduced by the second-order term does not necessarily have to be a hexagon. However, in agreement with experimental observations, a simple assumption is that both length scales are the same and therefore α increases linearly from zero with γ/β for $\gamma/\beta > 2$. In this case, the surface cells stretch to make the same contact area as cells in the bulk, and we can calculate the "covering ratio" for ordered 2D packings. Each bulk cell contacts a surface cell over a length $6L$ and therefore a surface cell covers approximately three bulk cells (see *SI Text*). The calculation for 3D is similar and the projected area of surface cells is 3.7 times greater than that of bulk cells.

Zebrafish Tissue Surface Cells. We investigate the covering ratio for the stretched surface cells in disordered 3D zebrafish ectoderm aggregates. We hand-segmented confocal slices as shown in Fig. 4 *A* and *B* from $n = 15$ aggregates to determine an estimate of the projected areas of each cell. The results are illustrated in Fig. 4*C*. The first observation is that stretched surface cells possess a preferred size that is reproducible from aggregate to aggregate, and there is a significant difference between surface cells and bulk cells. We find that the projected areas are 226 ± 100 μm^2 for the surface cells ($n_{\text{total}} = 236$) and 62 ± 9 μm^2 for the bulk cells ($n_{\text{total}} = 380$), i.e., the ratio between the projected areas is 3.7 ± 0.4, which is consistent with the theoretical prediction of 3.7. This stretching effect is not due to an increase in volume of surface cells, because using $V_{\text{cell}} \sim A_{\text{proj}}h$ (where h is the distance between the cell top and bottom), we find that bulk cells span on average 8–9 z slices and surface cells 3 slices, and A_{proj} for surface cells is about 3 times larger than for bulk cells.

What are the theoretical predictions for the surface tension in this case? We use the specific value for α that makes the contact

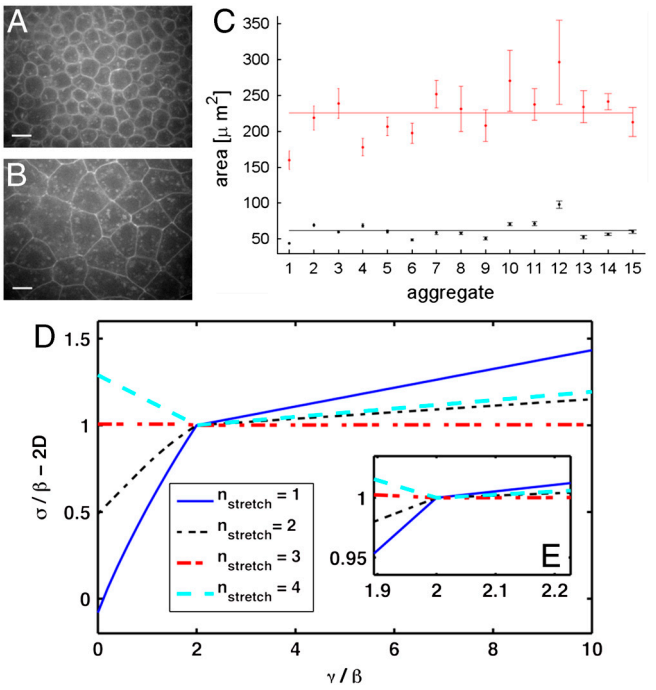

Fig. 4. (*A* and *B*) Representative confocal slices of a 3D zebrafish ectoderm aggregate in planes tangent to the aggregate surface. *A* intersects the surface cells, whereas *B* is at a depth of >25 μm and intersects a layer in the bulk. (Scale bar, 10 μm.) (*C*) Plot of the projected areas of all cells. Red points correspond to surface cells, whereas black points correspond to bulk cells, and the solid lines represent the mean of the entire dataset. Error bars represent errors on the aggregate mean. (*D*) Comparison of the relationship between σ, γ, and β as obtained from our extended model with $\alpha = \text{MAX}(0,(\gamma/2\text{-}\beta)/(2P_{\text{hex}}))$, for various surface cell configurations. The dash-dotted line corresponds to compact cell shapes, whereas the dashed and solid lines correspond to surface cells stretched over two or three cells, respectively. For $\gamma/\beta < 2$, compact cell shapes are optimal and the differential adhesion hypothesis is approximately satisfied, whereas for $\gamma/\beta > 2$, cells stretched over three interior cells are optimal and cortical tension dominates. (*E*, *Inset*) Magnification of crossover behavior in *D*.

length for bulk and surface cells equal and calculate the surface tension of ordered 2D aggregates for a wide range of values of γ/β and n_{stretch}. The experimentally observed surface tension and surface cell shape will correspond to the minimum solution at each value of γ/β. For $\gamma/\beta < 2$, compact surface cell shapes are optimal (solid line in Fig. 4*D*), whereas for $\gamma/\beta > 2$ the surface cells stretch across three interior cells (dash-dotted line in Fig. 4*D*). The surface tension exhibits a crossover at $\gamma/\beta \sim 2$ from adhesion-dominated behavior (DAH) to a dependence on the cortical tension and other mechanical effects.

Discussion

This work has two main implications. The first is that when $\gamma/\beta < 2$, surface cells do not stretch out and the differential adhesion hypothesis is essentially correct: Surface cells make fewer adhesive contacts than interior cells and this effect is the primary contribution to the surface tension, just as in fluids. Even though cells change shapes, the surface tension given by the magenta stars in Fig. 2*A* varies almost linearly with the *effective* adhesion. Our framework clarifies that "adhesion" as specified in the DAH must correspond to the net energetic contribution of contacting surfaces, which depends on both the free energy of cadherin binding complexes as well as local changes to the cortical tension induced by those bonds. Furthermore, the balance between cortical tension and adhesion is critical for determining surface cell shapes.

The second implication is that the analogy to fluids breaks down when surface cells stretch to make more nearest neighbor

contacts. In contrast to fluids, if surface cells stretch to have the same net contact perimeter as cells in the bulk, there is no adhesive contribution to the surface tension and the DAH must fail. This observation does not depend on a particular model. We have shown that, in high adhesion zebrafish aggregates, surface cells posses a well-defined, reproducible cross-sectional area that is significantly larger than that for bulk cells. Furthermore, this areal fraction is consistent with the assumption that surface cells are making the same surface area of contact in the bulk. Therefore we do not expect the surface tension of these aggregates to depend strongly on the adhesion.

The observation that stretched surface cells exist also leads us to consider cadherin diffusion. In our model, the adhesive energy density is constant along contacting interfaces, and therefore in stretched cells cadherin molecules must diffuse to the (much larger) contact interface to maintain the same density. However, in compact surface cells extra cadherins do not migrate to the contact interface. As discussed in the *SI Text*, this is a reasonable first approximation because there are no excess cadherins to bind with on the surface of the bulk cells, and therefore compact cells get no energy benefit from such a migration. However, heterogeneities in cadherin density could lead to unique minimum energy cell shapes and investigating these interactions is an avenue for future research.

Can these observed stretched surface cell states be explained by a minimal model? In a regime where adhesion is stronger than cortical tension, we show that stretched surface cells are the minimum energy structures as long as there is a restoring force that regulates the areas of cells in contact. Although there are at least two plausible mechanisms for such a restoring force, adhesion molecule regulation and elasticity of the cortical network, our experiments have not directly tested these assumptions. In addition, when calculating the surface tension shown in Fig. 4*D* and *E*, we chose a particular value for the magnitude of this restoring force (α) based on the assumption that the contact area preferred by the restoring force is the same as that for bulk cells with sharp corners. If this assumption is relaxed, the surface tension would still exhibit a crossover at $\gamma/\beta = 2$, but the exact nature of the crossover would change. Both the existence and the magnitude of the restoring force could be investigated in a future experiment using laser ablation to destroy individual cell–cell interfaces in low and high adhesion aggregates and analyzing the structural relaxation. Farhadifar et al. (23) have suggested that the anisotropy of the network response and the magnitude of the structural relaxation can be used to extract the relative magnitudes of cortical elasticity compared to interfacial tension.

For a model that includes only adhesion and cortical tension (Eq. **1**), stretched surface cells are not the minimal energy structures as shown in Fig. 4 *D* and *E*. Despite this, as γ/β approaches two, the energies of stretched states become closer to that for the unstretched states and active processes would allow surface cells to explore these "metastable" configurations. However, we would expect metastable stretched states to have a wide range of projected areas, weighted toward smaller area ratios because these have lower energy. The fact that zebrafish surface cells have a specific, reproducible area fraction significantly greater than unity suggests that these structures are not metastable, but instead have a preferred contact area with other cells as generated by the model described by Eq. **3**.

In order to fully interpret the available experimental data in the context of this model, we would like to compare the magnitude of the adhesive tension to that of the cortical tension in individual cells. However, the net effect of adhesive contacts on interfacial tension (which we denote γ) depends both on the free energy of adhesive molecule bonds and also on changes to the cortical tension along the contacting interface. Therefore it is difficult to determine how changes to the expression levels or activity of cadherins, actin, or myosin affect γ. In a recent study, Foty and Steinberg showed that surface tension increases linearly with the numbers of surface cadherins (18), in agreement with the DAH and our model if γ/β increases linearly with the number of cadherins. However, because the interaction between actin and cadherin-mediated adhesion is a highly dynamic process that is regulated by α-catenin (29, 30), it is possible to argue that increasing cadherin expression significantly increases cortical tension and γ/β remains unknown. Similarly, when we down-regulate surface tension by cytoskeletal drugs, both cortical tension *and* adhesive energy are decreased because cadherin bonds are stabilized by the cortical network (31–33). One attempt to dissect the connection of cortical tension and adhesion of individual cells was reported by Krieg et al. (19) using AFM measurements. Although in principle AFM is a promising technique for those measurements, thermal drift remains a technical challenge preventing long timescale measurements. The results presented in (19) are on timescales of seconds and therefore too short to be relevant for the interpretation of tissue surface tension, which becomes valid only for long timescales on the order of tens of minutes. At these short timescales, the actin network does not remodel (34, 35) and the AFM probes the cytoskeleton elasticity and not exclusively the cortical tension. In addition, cadherin bonds strengthen significantly over time after initiation, so the adhesion dynamics over long timescales are different from those on short timescales (16, 31, 32).

We propose a set of experiments to evaluate the cortical-tension β and the effective adhesion γ. One possible approach for measuring the cortical tension is micropipette aspiration (27, 33). Also, in the near future it may be possible to reduce AFM drift enough to perform single-cell AFM experiments on the relevant long timescales, allowing one to measure the repulsive force generated by the bare cortical tension. The determination of the effective adhesion γ is more difficult. A semiquantitative approach for studying the effect of γ/β would be the use of cell lines that are engineered to express a controlled number of fluorescently labeled adhesion molecules, actin, myosin, and actin-associated proteins as done previously for Madin–Darby canine kidney cells by Yamada and Nelson (36). One could then quantify tissue surface tension and surface cell geometries as a function of the ratio of the densities of these molecules and investigate the predicted crossover in surface cell shapes and energy contributions at $\gamma/\beta = 2$ in our model. Second, laser ablation experiments can be used to estimate the interfacial tension along cell–cell interfaces (23). Additionally, it would be interesting to adapt the shape-energy functional given by Eq. **1** to a Monte Carlo or Cellular Potts model (26, 37) approach with activated dynamics and compare simulated cell sorting based on this interaction potential with the experimentally available data.

These approaches are an avenue of future research, and for the present our model suggests that surface cell shapes can be used to estimate the ratio between adhesion and cortical tension in an experimental aggregate.

Disordered cellular structures appear in many problems in physics and biology; the fact that one can calculate an analytic expression for their surface energy (Fig. 2 *A* and *B*) is surprising and useful. For example, Eq. **1** with $\gamma = \beta$ describes a dry foam and therefore our method can be used to calculate the surface energies of finite 2D foams as a function of cluster size. A simple extension of this work also predicts how cells in the bulk change shape from spheres (when there is no adhesion) to polyhedra with sharp corners when the adhesion is high (see *SI Text*).

We have developed a minimal model that relates tissue surface tension to the mechanical properties of individual cells, such as cortical tension, cell–cell adhesion, and incompressibility. Our model suggests how a crossover from the DAH to significant cortical-tension dependence might occur, which is an important consideration when designing drugs to alter mechanical behavior. Both the DAH and the DITH were developed to explain cell sorting experiments in vitro. Integrating both surface tension-based

hypotheses into a single framework, our model predicts not only that cells sort out according to the surface tension of their aggregates but also that this surface tension exhibits a crossover from a regime where intercellular adhesion is the dominant contributor to one where cortical tension dominates.

Methods

Generation of Zebrafish and *P*-Cadherin Expressing L-Cells Aggregates. Zebrafish aggregates were generated as previously described in refs. 1 and 5. Mouse embryonic fibroblast L929 cells were cotransfected by electroporation with plasmids encoding *P*-cadherin and G418 resistance, as previously described (18). Detailed procedures are described in the *SI Text*.

Fluorescent Microscopy. For structural studies and antibody staining, zebrafish cell aggregates were imaged on an Olympus spinning disc microscope at room temperature using 10 and 20× air or 40 and 60× oil objectives. Actin expression was assessed by phalloidin staining (1:100; Invitrogen) and E-cadherin was identified by antibody staining (1:750) (38) as described in ref. 39.

In the *SI Text*, to show the motion of surface cells in and out of the bulk, zebrafish ectoderm aggregates, labeled with histone-conjugated Alexa488, were imaged on a two-photon microscope using a 40× water immersion objective. In situ hybridization was carried out as described in refs. 1 and 5, and imaged using a Leica MZ16FA microscope.

Scanning Electron Microscopy. Cell aggregates were fixed for 1 h with 2.5% electron microscopy grade glutaraldehyde in 0.15 M cacodylate buffer, pH 7.4, at room temperature. They were washed 3× for 10 min with the buffer and dehydrated in a closely graded 50–100% ethanol series stored at 20° for 5-min intervals. They were then transferred through two more changes of ice-cold 100% ethanol for 20 min, washed 2× for 10 min with amyl acetate, air dried at room temperature, sputter-coated with gold, and examined in the SEM.

Determination of Projected Surface Area. Projected surface areas of surface and bulk cells in cell aggregates were determined using a built-in ImageJ (version 1.4, National Institutes of Health image) routine. The obtained area pixel counts were imported into Matlab and analyzed as well as plotted. For bulk cells, five neighboring planes, 3 μm apart, were compared. We analyzed only cells that were clearly visible in the equatorial plane. The maximum area of each cell was then measured. For surface cells, the problem of not being in the maximum plane does not exist therefore we analyzed only three planes. We concentrated on the surface in the middle of the field of view where the curvature of the aggregate would not significantly distort the cell shapes. We analyzed 15 aggregates from three experimental days and generated a dataset of 236 surface and 380 bulk cells.

Tissue Surface Tensiometry. Tissue surface tensiometry was carried out as previously described (1–3, 5). From the force and the shape of the aggregate before and under compression at force equilibrium, tissue surface tension was calculated as described in ref. 1.

In Silico Generation and Analysis of 2D Cellular Structures. Standard methods (40, 41) were used to generate a 2D random, soft sphere packing with periodic boundary conditions and a box size L. A voronoi tessellation of the soft sphere packing was constructed using Matlab, restricted to particles with a center of mass within $0.4L$ of a randomly chosen point in the packing. This tessellation generates a finite, connected cellular structure composed of N cells which was then used as an input to the program "Surface Evolver," by Brakke (28), which numerically minimizes the total perimeter of the entire cellular structure, under the constraint that the area of each cell should equal the average area. Each interior edge of the cell was initialized with a tension unity and each surface edge was initialized with a tension $(\beta/(2\beta-\gamma))$. See *SI Text* for additional details.

ACKNOWLEDGMENTS. The authors thank J. A. Talbot, S. Thiberge, and the imaging core facility for the two-photon movie, S. F. Norrelykke, W. Ellenbroek, and B. Chen for scientific discussions, and T. Newman and S. F. Norrelykke for reading various versions of the manuscript.

1. Schoetz E-M (2008) *Dynamics and Mechanics of Zebrafish Embryonic Tissues—A Study of the Physical Properties of Zebrafish Germlayer Cells and Tissues and Cell Dynamics During Early Embryogenesis* (Verlag Dr. Mueller Publishing Group, Saarbruecken).
2. Foty RA, et al. (1994) Liquid properties of embryonic tissues: Measurement of interfacial tensions. *Phys Rev Lett* 72(14):2298–2301.
3. Foty RA, et al. (1996) Surface tensions of embryonic tissues predict their mutual envelopment behavior. *Development* 122(5):1611–1620.
4. Forgacs G, et al. (1998) Viscoelastic properties of living embryonic tissues: A quantitative study. *Biophys J* 74(5):2227–2234.
5. Schoetz EM, et al. (2008) Quantitative differences in tissue surface tension influence zebrafish germlayer positioning. *HFSP J* 2(1):1–56.
6. Mgharbel A, Delanoë-Ayari H, Rieu J-P (2009) Measuring accurately liquid and tissue surface tension with a compression plate tensiometer. *HFSP J* 3:213–221.
7. Norotte C, Marga F, Neagu A, Kosztin I, Forgacs G (2008) Experimental evaluation of apparent tissue surface tension based on the exact solution of the Laplace equation. *Europhys Lett* 81:46003.1–46003.6.
8. Davis GS, Phillips HM, Steinberg MS (1997) Germ-layer surface tensions and "tissue affinities" in Rana pipiens gastrulae: Quantitative measurements. *Dev Biol* 192:630–644.
9. Guevorkian K, Colbert M-J, Durth M, Dufour S, Brochard-Wyart F (2010) Aspiration of biological viscoelastic drops. *Phys Rev Lett* 104(21):218101.
10. Armstrong PB (1989) Cell sorting out: The self-assembly of tissues in vitro. *CRC Cr Rev Biochem Mol Biol* 24:119–149.
11. Holtfreter J (1944) A study of the mechanics of gastrulation. *J Exp Zool* 95:171–212.
12. Steinberg MS (1996) Adhesion in development: An historical overview. *Dev Biol* 180 (2):377–388.
13. Foty RA, Corbett SA, Schwarzbauer JE, Steinberg MS (1998) Effects of dexamethasone on cadherin-mediated cohesion of human fibrosarcoma HT-1080 cells. *Cancer Res* 58:3586–3589.
14. Foty RA, Steinberg MS (1997) Measurement of tumor cell cohesion and suppression of invasion by E- or P-cadherin. *Cancer Res* 57:5033–5036.
15. Duguay D, Foty RA, Steinberg MS (2003) Cadherin-mediated cell adhesion and tissue segregation: Qualitative and quantitative determinants. *Dev Biol* 253(2):309–323.
16. Borghi N, Nelson JW (2009) Intercellular adhesion in morphogenesis: Molecular and biophysical considerations. *Curr Top Dev Biol* 89(1):1–32.
17. Lecuit T, Lenne PF (2007) Cell surface mechanics and the control of cell shape, tissue patterns and morphogenesis. *Nat Rev Mol Cell Biol* 8:633–644.
18. Foty RA, Steinberg MS (2005) The differential adhesion hypothesis: A direct evaluation. *Dev Biol* 278(1):255–263.
19. Krieg M, et al. (2008) Tensile forces govern germ-layer organization in zebrafish. *Nat Cell Biol* 10(4):429–436.
20. Harris AK (1976) Is cell sorting caused by differences in the work of intercellular adhesion? A critique of the Steinberg hypothesis. *J Theor Biol* 61(2):267–285.
21. Brodland GW (2003) New information from aggregate compression tests and its implications for theories of cell sorting. *Biorheology* 40:273–277.
22. Graner F (1993) Can surface adhesion drive cell-rearrangement? Part I: Biological cell-sorting. *J Theor Biol* 164:455–476.
23. Farhadifar R, et al. (2007) The influence of cell mechanics, cell-cell interactions, and proliferation on epithelial packing. *Curr Biol* 17:2095–2104.
24. Paluch E, Heisenberg C-P (2009) Biology and physics of cell shape changes in development. *Curr Biol* 19(17):R790–R799.
25. Hufnagel L, et al. (2007) On the mechanism of wing size determination in fly development. *Proc Natl Acad Sci USA* 104(10):3835–3840.
26. Graner F, Glazier JA (1992) Simulation of biological cell sorting using a two-dimensional extended Potts model. *Phys Rev Lett* 69(13):2013–2016.
27. Evans E, Yeung A (1989) Apparent viscosity and cortical tension of blood granulocytes determined by micropipet aspiration. *Biophys J* 56(1):151–160.
28. Brakke KA (1992) The surface evolver. *Exp Math* 1(2):141–165.
29. Drees F, et al. (2005) [alpha]-Catenin is a molecular switch that binds E-cadherin-[beta]-catenin and regulates actin-filament assembly. *Cell* 123(5):903–915.
30. Yamada S, et al. (2005) Deconstructing the cadherin-catenin-actin complex. *Cell* 123 (5):889–901.
31. Imamura Y, et al. (1999) Functional domains of alpha-catenin required for the strong state of cadherin-based cell adhesion. *J Cell Biol* 144(6):1311–1322.
32. McClay DR, Wessel GM, Marchase RB (1981) Intercellular recognition: Quantitation of initial binding events. *Proc Natl Acad Sci USA* 78(8):4975–4979.
33. Chu Y-S, et al. (2004) Force measurements in E-cadherin-mediated cell doublets reveal rapid adhesion strengthened by actin cytoskeleton remodeling through Rac and Cdc42. *J Cell Biol* 167(6):1183–1194.
34. Adams CL, James Nelson W, Steven J Smith (1996) Quantitative analysis of cadherin-catenin-actin reorganization during development of cell-cell adhesion. *J Cell Biol* 135:1899–1911.
35. Angres B, Barth A, Nelson WJ (1996) Mechanism for transition from initial to stable cell-cell adhesion: Kinetic analysis of E-cadherin-mediated adhesion using a quantitative adhesion assay. *J Cell Biol* 134(2):549–557.
36. Yamada S, Nelson WJ (2007) Localized zones of Rho and Rac activities drive initiation and expansion of epithelial cell-cell adhesion. *J Cell Biol* 178(3):517–527.
37. Mombach JCM, et al. (1995) Quantitative comparison between differential adhesion models and cell sorting in the presence and absence of fluctuations. *Phys Rev Lett* 75 (11):2244–2247.
38. Babb S, et al. (2001) Zebrafish E-cadherin: Expression during early embryogenesis and regulation during brain development. *Dev Dyn* 221:231–237.
39. Köppen M, et al. (2006) Coordinated cell-shape changes control epithelial movement in zebrafish and Drosophila. *Development* 133:2671–2681.
40. Durian DJ (1997) Bubble-scale model of foam mechanics: Melting, nonlinear behavior, and avalanches. *Phys Rev E* 55:1739–1751.
41. O'Hern CS, et al. (2002) Random packings of frictionless particles. *Phys Rev Lett* 88 (7):075507.1–075507.4.

Supporting Information

Manning et al. 10.1073/pnas.1003743107

SI Text

SI Methods. ***Zebrafish cell aggregate preparation.*** In brief, wildtype zebrafish embryos were injected at one-cell stage with lefty mRNA (50 pg) or Cyclops mRNA (100 pg) and a fluorescent dye (Invitrogen). For adhesion down-regulation, 6–8 ng of E-cadherin morpholino or N-cadherin morpholino (Gene Tools, LLC) was coinjected with the mRNA and fluorescent dye as described previously (S1). For the structural studies, Gap43-GFP (100 pg) was coinjected as a membrane marker and Hoechst staining (50 μg/mL) was used in some cases to mark the cell nuclei. For the two-photon imaging and antibody staining, histone conjugated Alexa 488 was used as a cell nucleus marker. Aggregates were generated mechanically at sphere-to-sphere oblong stage and then transferred into CO_2-independent cell-culture medium (Gibco, Invitrogen), supplemented with 10% FCS and antibiotics (S1, S2).

Cell death staining. Zebrafish aggregates were incubated in propidium iodide (1:1,000) for at least 30 min before imaging.

Generation of P-cadherin expressing L-cell aggregates. Mouse embryonic fibroblast L929 cells were cotransfected by electroporation with plasmids encoding P-cadherin and G418 resistance, as described previously (S3). Briefly, 3×10^6 cells were suspended in 300 μL of transfection medium (RPMI medium 1640, 0.1 mM DTT, 10 mM dextrose). Twenty micrograms of PβactPcad (S4) and 2 μg of pcDNA3 (Invitrogen) cDNA were electroporated at 200 V and 960 μF in a 0.4-cm electroporation cuvette using a Biorad Gene Pulser II apparatus. Transfected cells were plated into 100-mm tissue culture plates, grown for 24 h, whereupon they were selected in 800 μg/mL of G418 until resistant cells reached 40–50% confluence. Resistant cells were screened for P-cadherin expression by flow cytometry. Cells were detached with trypsin-calcium (Gibco-BRL), washed three times in HBSS then incubated in 10 μg/mL anti-P-cadherin antibody (PCD-1, Zymed) on ice for 45 min. Cells were again washed with cold HBSS and incubated on ice for an additional 45 min with an Alexafluor-488-conjugated goat-anti-rat secondary antibody (Zymed). Cells expressing P-cadherin were sorted by FACS (Epics Altra, Beckman Coulter), expanded then subjected to limiting dilution cloning. Two clonal cell lines were generated, each expressing a different level of P-cadherin, which we designate as LP1a and LP2. Spheroidal aggregates were prepared using the hanging drop method. Near-confluent monolayers were dissociated from 10-cm tissue culture plates with trypsin/EDTA. Dispersed cells were washed in complete medium to inhibit the trypsin, then centrifuged to pellet the cells. The pellets were washed with PBS and resuspended in complete medium at a concentration of 2.5×10^6 cells/mL. Ten microliter aliquots of cell suspension were deposited on the underside of the lid of a 10-cm tissue culture dish. The bottom of the dish contained 5 mL of PBS and served to prevent evaporation of the drops by forming a hydration chamber. Hanging drops were created by inverting the lid over the hydration chamber. The drops were incubated at 37 °C, 5% CO2, and 95% humidity for 2 days allowing cells to coalesce and form aggregates. At day 2, aggregates were transferred to 10-mL shaker flasks (BellCo Glass) in 3-mL complete medium and placed in an orbital shaker at 110 rpm for another 1–2 days.

Rescue of cytochalasin D-treated aggregates. Mouse fibroblast L cells were transfected for expression of N-cadherin as previously described (S5). After selection in G418 and limiting dilution cloning, one cell line, LN77S1, was expanded and used to generate spherical aggregates for tissue surface tensiometer (TST) measurements. For cytochalasin D (CD) treatment, aggregates were generated by the hanging drop method, whereupon they were treated for 15 min in 2 μg/mL CD (Sigma) and subjected to TST (in CD-containing compression medium), as previously described. After TST measurements, aggregates were removed from the TST compression chamber and placed in fresh medium without CD for 2 h, whereupon they were subjected to another round of TST, now in the absence of CD.

In silico analysis of random 2D cellular structures: Surface Evolver details. A voronoi tessellation was generated as discussed in *Methods* of the main text and used as an input to the program "Surface Evolver," by Brakke (S6), which numerically minimizes the total perimeter of the entire cellular structure, under the constraint that the area of each cell should equal the average area. Each interior edge of the cell was initialized with a tension 1, and each surface edge was initialized with a tension $\beta/(2\beta - \gamma)$. The minimization routine uses gradient descent to find a local minimum (i.e., there are no positive energy changes permitted). Surface Evolver was used in two-dimensional "STRING" mode, with an autochop value of 0.186 in units where the polygons are of unit area, to ensure that the maximum line segment was $l_{\max} = 0.3L$, where $L = 0.62$ is the length of a side of a regular hexagon with unit area. In addition, the fixed scale factor was set at 1.73×10^{-4} to ensure resolution of lengths $l_{\min} = 0.1 \times l_{\max} = \sqrt{2 \times \text{scale factor}}$. We have verified that altering the scale factors slightly does not significantly alter the results, and reducing the scale factors significantly drastically increases the computing time.

The resulting structure was minimized using 1×10^5 gradient descent steps. In all cases, this is a sufficient number of steps so that the energy changes by less than one part in 10^5, and we have also verified that increasing the number of steps does not change the result. The resulting structures were analyzed in Matlab. Surface interfaces are easily identifiable because they are not shared, and the surface perimeters were calculated. The projected lengths of surface interfaces were calculated by identifying the end points of surface interfaces and calculating the Euclidean distance between them. For each data point for the ratio γ/β, this process was repeated for six random initial conditions with 185 ± 15 cells. We also studied a larger structure with 449 cells and found that the surface tension varied by less than 2% from the smaller aggregates.

Supplemental Experimental Data. Figs. S1 and S2 show results from control experiments that were carried out to confirm (*i*) that stretched surface cells are not changing cell type and become epithelial like, (*ii*) that treatment of cell aggregates with cytoskeletal drugs is reversible and does not harm the cells, (*iii*) rounded surface cells are viable and do not express any death marker, and (*iv*) sort in hanging drop experiments.

Calculation of Surface Tension from the Mechanical Model. Surface tension is the difference in mechanical energy between surface cells and interior cells times the number of cells per unit surface area. The number of cells per unit area is equal to unity divided by the projected area A_{proj} (or projected length in 2D) of a single cell onto the surface of the aggregate, and we recall Eq. **2** from the main text:

$$\sigma \equiv \left(\frac{\Delta W}{\text{one cell}}\right)\left(\frac{\text{one cell}}{A_{\text{proj}}}\right). \qquad \textbf{[S1]}$$

Using this definition for the surface tension and the mechanical energy given in the main text (Eq. **1**), we can determine the surface tension for various cell geometries in two and three dimensions.

Two-dimensional ordered structure analysis, $n_{stretch} = 1$. Our starting point will be a perfectly ordered 2D hexagonal lattice of cells as shown in Fig. 1*D* in the main text. This structure satisfies force balance everywhere and is the minimum energy structure in an infinite plane.

Recall the expression for the mechanical energy of a single cell as a function of the adhesive energy per unit area γ and the cortical tension β, which is Eq. **1** in the main text:

$$W = -\frac{\gamma}{2}P_c + \beta P_T. \qquad \textbf{[S2]}$$

Then the energy W_{in} for a single cell in the interior of the aggregate is simply

$$W_{\text{in}} = -\frac{\gamma P_{\text{hex}}}{2} + \beta P_{\text{hex}} \quad |A = 1, \qquad \textbf{[S3]}$$

where $P_{\text{hex}} = 6L = 6\sqrt{2/(3\sqrt{3})} \sim 3.72$ is the perimeter of a hexagon with area $A = 1$. Our goal is to find the minimal energy ordered structure. Because the total area is constrained, we assume that the total energy is minimized when the surface energy is minimized subject to the area constraint. As discussed in *Stretched surface cells*, one can show that, for $\gamma < 2\beta$, the ordered structure that minimizes the surface energy is one where surface cells individually minimize their mechanical energy W subject to the constraint $A_{\text{tot}} = 3\sqrt{3}L^2/2$ and boundary conditions imposed by four neighboring cells. (See Fig. 1(*D*) in the main text.) For the remainder of this section, we focus on $n_{\text{stretch}} = 1$; the remaining possibilities are discussed in *Stretched surface cells*. Interfaces must have constant curvature because they are fluid and do not support a shear stress. Therefore it is possible to parameterize the cell shape in terms of two curves, L_{side} and L_{cap}, where L_{side} is a line of length $\tilde{L}_{\text{side}}L$, and L_{cap} is a circular segment of length $\tilde{L}_{\text{cap}}L$. The cell shape is therefore a pentagon plus a circular segment with chord length $\sqrt{3}L$.

Next, we use the following formula for the area A in terms of the circle radius R and segment height h:

$$A(R,h) = R^2\cos^{-1}\left(\frac{R-h}{R}\right) - (R-h)\sqrt{2hR-h^2}. \qquad \textbf{[S4]}$$

Similarly, the chord length can be written as

$$c(R,h) = 2\sqrt{2hR-h^2}. \qquad \textbf{[S5]}$$

The area of the circular segment is given by the difference between the total area $A_{\text{tot}} = 3\sqrt{3}L^2/2$ and the area of the pentagon:

$$A_{\text{circ}} = \left(\frac{3\sqrt{3}}{4} - \sqrt{3}\tilde{L}_{\text{side}}\right)L^2. \qquad \textbf{[S6]}$$

Substituting $c = \sqrt{3}L$ and $A = A_{\text{circ}}$, we nondimensionalize all lengths by L and solve numerically for R and the arc length $\widetilde{L_{\text{cap}}} = 2R\sin^{-1}(c/2R)$. $\tilde{L}_{\text{side}}$ must be less than 0.75 because $R = \infty$ at that point. In addition, L_{side} is bounded below by ~0.07, as $h = R = c/2$ at that point, and for smaller values of L_{side} packed cells begin to overlap. Next, we find the value of $\tilde{L}_{\text{side}}$ that minimizes the energy W for surface cells at a specified value of γ/β. Eq. **S1** can then be used to determine the surface tension:

$$\sigma = \frac{\gamma(\frac{3L}{2} - L_{\text{side}}) + \beta(-3L + 2L_{\text{side}} + L_{\text{cap}})}{\sqrt{3}L}. \qquad \textbf{[S7]}$$

A plot of the surface tension for the ordered aggregate as a function of γ and β is given by the dashed black line in Fig. 2(*A*) of the main text. One sees immediately that the surface tension increases with increasing adhesion. Because the plot is curved, there is a slight dependence on cortical tension, but this effect is weak. With $\gamma = \beta$, this model is equivalent to a foam, and these results can be compared to those of Fortes and Rosa (S7) who determine the surface energy of a disordered foam via a different method. Although Fortes and Rosa incorrectly identify the spherical cap as a full hemisphere, this does not introduce a larger error and therefore their predictions for the surface tension of ordered structures is similar to ours. This calculation is valid for $0.186 < \gamma/\beta < 2$. The upper bound is the point at which bulk cells begin to stretch out beyond hexagons, as discussed in *Stretched surface cells*. The lower bound is the point at which gaps begin to open up between bulk cells.

Rounding of interior cells. It is obvious that in the limit of zero adhesion, the minimum energy mechanical state for cells should be spheres (3D) or circles (2D). However, in our model [and many other models (S8, S9)], the bulk cells are approximated as polyhedra or polygons. How do the cell structures transition from spheres to polyhedra as the adhesion increases?

Here we show that in our simple-ordered 2D model there is a *continuous* transition from a state where the cells have a packing fraction of unity (i.e., they fill space for $\gamma/\beta > 0.186$) to a state where gaps open up between cells and the cells become rounded $\gamma/\beta < 0.186$. Therefore, for systems with negligible contributions from elasticity or bending energies, the assumption that the cells are polygonal (as in refs. S8, S9) is exact as long as $\gamma/\beta > 0.186$. We expect a similar result to hold in 3D.

In the ordered system, symmetry, and force balance requires that the minimum energy shape be a hexagon with "rounded corners" as illustrated in Fig. S3*A*. The edges of the hexagon are length L, whereas the radius of the circle that defines the corners is denoted R. Because cell area is conserved, L can be viewed as a function of R:

$$L(R) = \frac{\sqrt{2}}{3}\sqrt{\sqrt{3} + (6 - \sqrt{3}\pi)R^2}. \qquad \textbf{[S8]}$$

Then one can write the total mechanical energy of the cell W as a function of $L(R)$ and R, and take the derivative with respect to R to find the minimum. A plot of $W(R)$ as a function of γ/β is shown in Fig. S3*B*.

For $0 < \gamma/\beta < 0.186$, the minimum of $W(R)$ occurs at a number $R^* > 0$. For $\gamma/\beta = 0$, $R^* = 0.564$, which corresponds to a global shape which is a circle, as expected. At $\gamma/\beta \leq 0.186$, the minimum of $W(R)$ occurs at or below zero. Because $R < 0$ corresponds to convex shapes that do not tile the plane, these solutions are unphysical. Then the minimum energy packing is $R = 0$, and the global minimum energy shapes are polygonal (see Fig. S3*C*).

The above analysis was based on a cell mechanical energy with no elasticity (i.e., Eq. **1** in the main text.) However, when $\gamma/\beta > 2$, we introduce an elastic term that acts as a restoring force to prevent cells from increasing their perimeter (Eq. **3** in the main text). Why don't we include an elastic term for $\gamma/\beta < 2$? Because it is not consistent with our images of bulk cells.

To understand this, we first note that, in the aggregates we imaged, the cells in the interior are shaped as polyhedra, with no discernible rounding at the corners. We could imagine adding an elastic term to the mechanical energy, even for $\gamma/\beta < 2$:

$$W = -\frac{\gamma}{2}P_c + \beta P_T + \alpha P_c^2. \qquad \textbf{[S9]}$$

We now analyze this energy in the same way as before. Fig. S3*D* is a plot which shows the rounding of the edges R as a function of γ/β, for different values of the elasticity parameter α. The lowest curve corresponds to $\alpha = 0$ and is therefore exactly the same as Fig. S3*C*. If the elasticity is zero, then this regime is very small ($0 < \gamma/\beta < 0.18$). But as the elasticity increases, there is a larger and larger regime where bulk cells are rounded.

If the adhesion is greater than the cortical tension (i.e., negative line tension) then it is possible to choose an elastic constant $\alpha > 0$ so that bulk cells always remain polyhedral (i.e., the corners are sharp.) In fact, this is how we chose α for $\gamma/\beta > 2$. As discussed in the main text, this means that the elasticity coefficient α rises linearly from zero in γ/β for $\gamma/\beta > 2$.

This analysis suggests that when a second-order elastic term is added to the cell mechanical energy (as Eq. **3** in the main text), there is a large regime where the interior cells are quite rounded, which is not consistent with a vertex model. In some biological tissues, such as epithelial layers, there are additional processes and structures (such as focal adhesions) that ensure gaps do not open up between cells. Vertex models implicitly include these processes as a constraint on tissue structure, but it is not clear that such a constraint is appropriate for cell aggregates. Determining when such a "vertex energy" is important for various tissue types is an interesting avenue for future research.

Disordered two-dimensional structures. Active processes allow cells to exchange neighbors and explore many possible configurations, so that they are not confined to the global minimum energy configuration. Instead, the collection of cells explore a large number of local minima, and these configurations are disordered, much like the typical configurations of a fluid or a jammed granular material. We now use numerical simulations to show that the surface tension for 2D disordered aggregates is related in a remarkably simple way to that for ordered structures, and make a conjecture about 3D aggregates.

First, we used the Surface Evolver program developed by Brakke (S6) to numerically find the local minimum energy 2D structures for various random initial conditions and values of γ/β (see *Methods*). The fact that there must be exactly six cells with a different number of neighbors (called isolated disclinations) is a consequence of the "Gauss-Bonnet" theorem, which can also be used to understand features of random aggregates. For example, one can show that the average number of nearest neighbors must be six in the bulk and four on the boundary, except for those six disclinations. As shown in Fig. S4, cells in a random aggregate which do not have the average number of nearest neighbors can be grouped into "defect pairs," where the pair has the correct average. These defect pairs that occur both on the surface and in the bulk should have a different energy W and a different geometry L_{proj} from the cells which have the average number of neighbors.

Fig. 2 *D* and *E* in the main text are two structures generated by Surface Evolver, where each cell is colored according to its number of neighbors. To understand how disorder changes the surface tension given by Eq. **S7**, one must ask if these defects alter the mechanical energy difference, ΔW or the projected length L_{proj}. By comparing the statistics of defect pairs and surface cells in numerical simulations, we find something surprising: At low values of γ/β, only L_{proj} changes, whereas at large values of γ/β, the changes in ΔW and L_{proj} offset, so that their ratio approaches unity.

Table S1 compares various properties of the cellular structures as a function of the ratio γ/β. The surface tension is calculated using Eq. **S1**. For surface cells, we compare the projected length and energy of defect pairs to those quantities for cells with four nearest neighbors. The percent difference between these projected lengths ($\%\Delta l_{\text{proj}}$), and energies ($\%\Delta W_{\text{surf}}$) are calculated. Similarly, we calculate the percent difference in energy between defect pairs and six-sided cells in the bulk ($\%\Delta W_{\text{int}}$). Perhaps surprisingly, the energies of defect pairs and average cells in the interior differ by less than 1%. For surface cells, the percent difference in the projected length is significantly larger than the percent difference in energy, an effect which is more pronounced at lower values of γ/β. For example, at $\gamma/\beta = 0.33$, the projected lengths differ by 9%, whereas the energies differ by only 0.2%. Thus, when the ratio γ/β is small, the primary effect of the defect pairs is to alter the geometry and not the energy, leading to a very simple *analytic* prediction for the surface tension of disordered aggregates. The projected length, which corresponds to the macroscopic perimeter of the entire aggregate, is the only parameter changed by the disorder in the limit of small γ/β. The total area cannot change, however, because the number of cells with fixed area is constant. Because the macroscopic shape of a 2D hexagonal ordered crystal has hexagonal symmetry, whereas the disordered structure is spherically symmetric, this suggests that the macroscopic perimeter should change as the ratio of the perimeter of a hexagon to a circle of the same area: $\sigma_{\text{rand}} = 1.05\sigma_{\text{ordered}}$. This amazingly simple ansatz is tested numerically in Fig. 2 *A* and *B* in the main text. The blue line is the theoretical prediction, whereas the magenta stars are numerical results from Surface Evolver. There is excellent agreement between the theory and numerical simulations, though there is a systematic deviation at large values of γ/β. This systematic deviation results from the fact that the geometry places a strict constraint on the macroscopic surface tension when $\gamma = 2\beta$. As illustrated in Fig. S5*C*, force balance is satisfied at all junctions between cells. As γ approaches 2β, the tension in cell–cell interfaces approaches zero and force balance requires that surface cells have a flat interface with the cell-culture medium. Then the macroscopic surface tension is identically the cortical tension. Because the *ordered* surface tension also approaches β as $\gamma \to 2\beta$, the surface tension of disordered aggregates must approach σ_{ordered} for large values of γ/β. This result also explains why the changes in ΔW and L_{proj} for defect pairs offset each other in this limit.

Fortes and Rosa use a different approach to calculate the surface energy of a disordered dry foam (S7), and because they perform an averaging over surface angle with a uniform measure, they predict that the surface energy is constant as a function of cluster size. As described above, our prediction for 2D disordered foams is for the large cluster limit, because we assume that the number of isolated disclinations (S6) is small compared to the total number of cells on the surface. However, our method can be extended to calculate the (higher) energy of surface cells that are disclinations. Accordingly, smaller clusters have larger surface tensions (analogusly to the Gibbs Thomson effect in fluids), and we can use our model to predict the dependence of surface energy on cluster size. If this 2D analysis extends to 3D, it might play an important role in determining timescales for cell sorting experiments.

Three-dimensional cellular structures. Although the 2D model is useful for developing tools and intuition, cell aggregates used in surface tension and cell sorting experiments cannot be approximated by two-dimensional structures. Here we sketch the results for three-dimensional ordered packings.

The minimal energy structure for an infinite packing of *identical* cells in 3D is the Kelvin cell or tetrakaidecahedron, which has eight hexagonal surfaces and six rhomboid surfaces. Weaire and Phelan (S10) have shown that there is another structure with different types of cells (though all the cells have the same volume) that has a lower energy, but we will restrict ourselves to identical ordered cells. We will also neglect the slight curvature of Kelvin cell faces, as these change the surface area by less than 1%. One can think of generating the Kelvin cell by placing spheres on a body-centered cubic (BCC) lattice and letting the spheres grow until they fill all space. A sphere on the BCC lattice has eight nearest neighbors which become the hexagonal interfaces,

and then six next-nearest neighbors which become the rhomboid interfaces.

By associating the Kelvin cells with their corresponding BCC lattice points, we can use crystal basis vectors to identifying facets of the finite cluster. Let [100], [010], and [001] be the three directions along the cube of the BCC lattice that generates the Kelvin cell packing. We will need to describe the minimum shape for a finite number of these cells. The surface of this three-dimensional "crystal" has two different types of faces that are composed of close-packed cells, which can be labeled [011] and [001] in crystallographic notation. Fortes and Rosa have shown that the minimum energy packing of a large number of ordered cells is a truncated rhombic dodecahedron with two types of faces, one of which is a rhombus with area A_{rhomb} oriented along [001] and symmetry-related directions and the other of which is a hexagon with area A_{hex} oriented along [001] and symmetry-related directions (S7).

First we will describe the minimum energy cell shapes that occur along each crystal facet. One can show that the cells on the surface normal to the [011] vector (and its symmetry-related cousins) have six nearest neighbors with hexagon contacts and four nearest neighbors with rhombus contacts. In contrast, cells on the surfaces normal to the [001] family of vectors have five nearest neighbors with rhombus contacts and four nearest neighbors with hexagon contacts. In both cases, the area of each rhombus is L^2 and the area of each hexagon is $3\sqrt{3}/2L^2$. The total volume of each cell is $V_K = 8\sqrt{2}L^3$, and the total surface area for Kelvin cells in the bulk is $SA_K = L^2 2(6\sqrt{3}+3)$. As in the two-dimensional case, let $\gamma/2$ be the adhesive energy and β the stretching energy per unit surface area. The compact surface cell shapes are a half-Kelvin cell, extended by a distance $x(\theta)$, and a cap of constant curvature. This 3D geometry is a much more complicated minimization compared to the 2D case, because the extension distance varies and the cap is not spherically symmetric. In general, this problem can only be solved numerically using Surface Evolver.

However, one can closely approximate the shapes by a combination of a polyhedral prism and a spherical cap. With these approximations and the constant volume constraint, it is again possible to parameterize the surface cell shapes in terms of two parameters, which correspond to the "side" surface area in contact SA_{side}, and the surface area of the cap SA_{cap}. The cap is constrained by requiring that its areal cross-section equal the areal cross-section of the Kelvin cell and its volume plus the volume of the extended Kelvin cell satisfy the total volume constraint $V = 8\sqrt{2}L^3$. We can then solve for the minimum energy shape, parameterized by x, as a function of the ratio γ/β. The energy is

$$\begin{aligned} W(x) &= -\frac{\gamma}{2}SA_{\text{side}} + \beta(SA_{\text{cap}} + SA_{\text{side}}) \\ &= \beta\left[\left(1-\frac{\gamma}{2\beta}\right)SA_{\text{side}}(x) + SA_{\text{cap}}(x)\right], \end{aligned} \quad \textbf{[S10]}$$

where the surface area of the cap is determined by $SA_{\text{cap}} = \pi(r_c^2 + h^2)$, $r_c = \sqrt{a/\pi}$ is the radius of the circular cross-section, and h is the height of the cap determined from $V_{\text{cap}} = 1/6\pi h(3r_c^2 + h^2)$. The cross-sectional area a and the cap volume $V_{\text{cap}}(x)$ are different for different orientations.

The difference in adhesive energy between exterior and interior cells is then given by

$$\Delta W_\gamma = -\gamma/2(SA^*_{\text{side}} - (1/2)SA_K); \quad \textbf{[S11]}$$

and the difference in stretching energy is

$$\Delta W_\beta = \beta(SA^*_{\text{cap}} + SA^*_{\text{side}} - (1/2)SA_K). \quad \textbf{[S12]}$$

As noted above, the functions $SA^*_{\text{cap}}(x)$ and $SA^*_{\text{side}}(x)$ must be calculated separately for the two planes [001] and [011]. First, we'll focus on cells oriented along the [011] plane. One can show that the areal cross-section, which is the projection of the cell onto the surface normal to [011], is an irregular hexagon with area $A_{011} = 4L^2\sqrt{2}$. The volume of the extended polyhedron is $4\sqrt{2}L^3 + 4\sqrt{2}L^2x$, and the volume of the cap is $4\sqrt{2}L^3 - 4\sqrt{2}L^2x$. The surface area that is in contact with other cells is $SA^{011}_{\text{side}} = L^2(6\sqrt{3}+3) + xL(4\sqrt{3}+2)$.

For cells oriented along the [001] plane, one can show that the cross-section is an irregular octagon with area $7L^2$. The perimeter is $L(4\sqrt{2}+4)$, and the contact area $SA^{001}_{\text{side}} = L^2(6\sqrt{3}+3) + Lx(4\sqrt{2}+4)$. The surface tension along each face is then $(\Delta W_\gamma + \Delta W_\beta)/A_{\text{proj}}$, evaluated at the minimum energy shape. A plot of the surface tension for both [001] and [011] crystal surfaces is given by the black and magenta dashed lines in Fig. 2*C* in the main text. The two lines lie on top of one another; the macroscopic surface tension is the same on each type of facet.

Because the macroscopic surface tension is the same along each interface as long as $\gamma < 2\beta$, we do not need to perform any averaging. However, when $\gamma > 2\beta$, surface cells stretch out, and we would like to calculate the global minimum energy shape for this system. In other words, we want to know the macroscopic dimensions of the crystal generated by packed Kelvin cells. To calculate A_{rhomb} and A_{hex}, we must determine the truncation length, d, that minimizes the 3D packing at a fixed volume, V^*. First, we rewrite the areas and total volume in terms of the truncation length d and the length of the original rhombic dodecahedron, l:

$$A_{\text{hex}} = \frac{2\sqrt{2}}{3}l^2\left[1 - 3\frac{d^2}{l}\right], \quad \textbf{[S13]}$$

$$A_{\text{rhomb}} = 4l^2\frac{d^2}{l}, \quad \textbf{[S14]}$$

$$V = \frac{16\sqrt{3}}{9}l^3\left(1 - 8\frac{d^3}{l}\right). \quad \textbf{[S15]}$$

The total surface energy E_{tot} of the packing is given by

$$E_{\text{tot}} = 12A_{\text{hex}}\gamma_{011} + 6A_{\text{rhomb}}\gamma_{001}, \quad \textbf{[S16]}$$

where γ_{011} and γ_{001} are the macroscopic surface tensions along each macroscopic crystal facet, and which we have shown above to be equivalent. We use the method of Lagrange multipliers to minimize E_{tot} as a function of d subject to the constant volume constraint. The energy E_{tot} is minimized at

$$d^* = l\left(\frac{2\sqrt{3}}{3} - \frac{\sqrt{6}}{3}\frac{\gamma_{011}}{\gamma_{001}}\right). \quad \textbf{[S17]}$$

Therefore $A_{\text{hex}} = 0.619l^2$ and $A_{\text{rhomb}} = 0.458l^2$. Later, we will need to find the average $\bar{q}$ of a quantity q that differs between different macroscopic crystal facets. To do so, one simply averages

$$\bar{q} = \frac{12A_{\text{hex}}\,q_{011} + 6A_{\text{rhomb}}\,q_{001}}{12A_{\text{hex}} + 6A_{\text{rhomb}}} \equiv 0.270\,q_{001} + 0.730\,q_{011}. \quad \textbf{[S18]}$$

Numerically solving for minimum energy surfaces for thousands of cells in 3D is beyond the scope of this work. However, we cautiously use the results for 2D disordered structures to make a conjecture about 3D random aggregates. First, force balance requires that surface tension must approach β in the limit that $\gamma/\beta \to 2$, so that the results for the ordered 3D packing should hold in this limit. Second, we suggest that at low values of γ/β, the surface tension is that for an ordered 3D aggregate

multiplied by the ratio between the surface area of a Kelvin cell and a sphere of the same area, $\sigma_{3\mathrm{Drand}} = 1.10\sigma_{3\mathrm{Dordered}}$.

An important prediction of this model is that the shapes of cells on the surface change as the surface tension changes. Fig. 2 *D* and *E* in the main text are numerical solutions for the minimum energy shapes of 2D cellular aggregates at two different values of γ/β. When γ/β is small (Fig. 2*D*), surface cells receive little energetic benefit from contacts compared to the energy they pay for stretching, and so their shape is rounded, which minimizes the total amount they have to stretch. In contrast, when γ/β is large (Fig. 2*E*), surface cells make as much contact with their neighbors as possible, resulting in stretched cells with a nearly flat cell-culture medium interface.

Stretched surface cells. In this section, we develop an expression for a second-order restoring force generated by adhesion molecule regulation. As discussed in the main text, another plausible restoring force is cortical elasticity, which would have the same form (S8, S9).

The adhesive energy per unit area in the bulk and the static size of the perimeter in contact are determined by the complicated equilibrium between surface and bulk cadherins as well as associated actin networks and myosin motors. Because these dynamics are constrained by the total number of such building blocks available in the cell, either (*i*) the contact area must be limited by these dynamics, or (*ii*) the adhesive energy per unit area must change. We believe that the first assumption is more relevant for our model, due to a specific feature of the adhesion dynamics. To form an adhesive interface, surface cadherins on one cell must bind to surface cadherins on another cell. Therefore it is not possible for two cells in contact to have different energy densities, and (*ii*) can only occur globally. Because we are interested in local changes to surface cells for fixed bulk properties, we use assumption (*i*).

Although this mean-field assumption is a good first approximation, it does not track the movement of individual cadherins, and heterogeneities could be important. For example, one could write down a model where the density of cadherins locally changes cell shape, and cell shape alters the density of cadherins, and then perform a global minimization to search for the optimal distribution of cadherins. The different dimerization states of cadherin molecules could also play an important role in cadherin–cadherin binding dynamics, as pointed out recently by Harrison et al. (S11).

With the assumption that the adhesive energy per unit area is constant, global adhesive molecule regulation would generate a restoring force that drives the contact length toward its equilibrium value. We can then write the adhesive energy W_{ad} as an expansion in $P_c - P_{\mathrm{pref}}$, where P_c is the actual size of the perimeter and P_{pref} is the equilibrium value:

$$W_{\mathrm{ad}}(P_c) = C_0 - C_2(P_c - P_{\mathrm{pref}})^2 + \mathcal{O}(P_c - P_{\mathrm{pref}})^3. \qquad \textbf{[S19]}$$

Adding Eq. **S19** to the cortical tension energy βP_T and keeping only first- and second-order terms, the total mechanical energy can be written

$$W = \left(-\frac{\gamma}{2} + \beta\right)P_c + \alpha P_c^2 + \beta\Delta P_T | A = 1, \qquad \textbf{[S20]}$$

where the term ΔP_T is the length of the cell perimeter not in contact with other cells, and α is related to P_{pref} and the second coefficient in the Taylor expansion. Because we are only interested in differences between energies, we define model parameters so that $W(P = 0) = 0$.

Importantly, we have now introduced a length scale P^* which is different from the length scale introduced by the incompressibility constraint, P_{hex}. To see this, note that in the bulk $P_T = P_c$. In this case, the mechanical energy functional is very similar to one used by Farhadifar et al. (S9) and Hufnagel et al. (S8). Neglecting the area constraint, W now has an equilibrium solution $P^* = (\gamma/2 - \beta)/(2\alpha)$.

However, for an infinite two-dimensional cellular structure, the minimal perimeter structure is a hexagonal lattice, with

$$P_{\mathrm{hex}} = 6\sqrt{2A/(3\sqrt{3})} \simeq 3.72.$$

Because we require a fixed area $A = 1$, the ground state of this functional under the area constraint is a perfect hexagonal network $P_{\mathrm{eq}} = P_{\mathrm{hex}}$ when $P^* < P_{\mathrm{hex}}$ and a soft network with $P_{\mathrm{eq}} = P^*$ for $P^* > P_{\mathrm{hex}}$, as pointed out by Farhadifar et al. (S9). In *Two-dimensional ordered structure analysis,* $n_{\mathrm{stretch}} = 1$, we assume that the bulk equilibrium is hexagonally packed, if and only if

$$(\gamma/2 - \beta)/(2\alpha) \leq P_{\mathrm{hex}}. \qquad \textbf{[S21]}$$

An interesting question is whether the inequality is saturated for embryonic tissues in the stretched limit. By comparing a similar model to laser ablation experiments, Farhadifar et al. (S9) found that 2D epithelial sheets were in a parameter regime that was far from saturating the inequality and the ground state was far from a soft network. This result is consistent with the observation that epithelial sheets behave more like an elasto-plastic solid than a liquid–cell rearrangements are rare and highly localized and the network has a strong elastic response.

However, zebrafish aggregates are more liquid-like, as the cells execute Brownian motion over intermediate timescales, aggregates fuse together, and the aggregate exhibits a surface tension. Therefore, we will assume that this inequality is saturated, so that cells on the surface minimize their energy when they have the same perimeter in contact as cells in the bulk. This choice has the additional benefit that α rises continuously from zero at $\gamma/\beta = 2$ so that the adhesion regulation only becomes important at large values of γ/β. Additionally this potential does not create an artificial elasticity at low values of γ/β, which matches the experimental observation of sharp corners in Fig. 1*A*.

It is obvious why this energy allows stretched surface states: The adhesion dynamics regulates the contact perimeter but not the total perimeter, so the surface cells prefer to have roughly the same contact perimeter (P^*) as cells in the bulk (P_{hex}) and they must stretch out to do so.

For surface cells, $P_T \neq P_c$, and the minimum energy *contact* perimeter, P_c^* is given by

$$P_c^* = \frac{1}{2\alpha}\left[\frac{\gamma}{2} - \beta\left(1 + \frac{d\Delta P_T}{dP_c}\right)\right], \qquad \textbf{[S22]}$$

where $d\Delta P_T/dP_c$ is the *additional* change in total perimeter caused by a unit change in contact perimeter. This quantity is roughly unity for a situation where a cell is just becoming unstable; the lowest energy perturbations are protrusions of vanishing volume and in this case an increase in the contact perimeter requires the same increase in the total perimeter.

Although contacts between cells in zebrafish aggregates are relatively smooth and cell shapes are polyhedral, the energy functional given by Eq. **S20** allows cells to increase their contact perimeter by roughening their boundary instead of stretching. A physical mechanism that prevents roughening is the bending stiffness of the membrane and cortical network, and this mechanical energy should be a function of the curvature of the cell interface. Including this term would require one to calculate spatial gradients of cell perimeters (instead of just lengths) and add a great deal of complexity to the model. Instead, we approximate this effect in our model by enforcing that interfaces are straight lines or circular arcs.

For large values of γ/β, the total energy (or, equivalently, the surface energy) of the cellular structure is minimized when surface cells stretch to make the same perimeter (or surface area in 3D) of contact as bulk cells. In this case, we would like to calculate the number of bulk cells that a surface cell touches, as illustrated in Fig. S5*A*. If we view the bulk cells as having a fixed shape, then we can calculate this "covering ratio" exactly for ordered packings. In 2D, each bulk cell contacts a surface cell over a length $2L$ and therefore covers exactly three bulk cells. However, the assumption that the bulk cells remain fixed as the surface cells stretch is clearly not correct; cells just beneath the surface relax slightly because they lose at least one vertex, inducing curvature and causing surface cells to spread out further. In addition, the above calculation neglects contacts between two surface cells, which will reduce the amount of contact surface cells must make with bulk cells.

For two-dimensional ordered systems, we can show that these effects cancel one another, and therefore the simple covering ratio approximation is reasonable. The force balance and area conservation constraints can be satisfied when surface cells are stretched over exactly an integer m number of bulk cells, as illustrated in Fig. S5*A*. (Although noninteger states are possible, they spontaneously break the symmetry of the ordered system and cannot be computed analytically.) In ordered case, bulk cells just underneath the surface either (*i*) remain hexagonal or (*ii*) possess a spherical cap of length $0.193L$. One can show that the contributions to the surface tension from these "second-layer" cells are of order $(m-1)(0.07)^2L^2\beta$ per cell and are negligible compared to the contributions from the exterior layer of stretched cells.

The surface tension can then be written

$$\sigma = \frac{(-\gamma/2 + \beta + 2\alpha P^*)\Delta P_c + \alpha \Delta P_c^2 + \beta \Delta P_T}{L_{\text{proj}}}, \qquad \textbf{[S23]}$$

where ΔP_c is the difference between the surface cell contact perimeter P_c^* and the perimeter in the bulk P^*. When α is chosen so that Eq. **S21** is an equality, the term which is first order in ΔP_c in Eq. **S23** is zero and the surface tension is

$$\sigma = \frac{\alpha \Delta P_c^2 + \beta \Delta P_T}{L_{\text{proj}}}. \qquad \textbf{[S24]}$$

After identifying the equilibrium shapes of the second-layer cells, we can then use the same techniques as in *Two-dimensional ordered structure analysis,* $n_{\text{stretch}} = 1$, to analytically solve for the stretched cell shapes that minimize the surface energy given by Eq. **S24**. Again, L_{side} is the contact length between cells at the surface, and L_{cap} is the length of the circular cap in contact with cell-culture medium. The minimum energy solutions for several values of m are shown in Fig. S6*A*.

Just as before, we calculate the surface tension as a function of γ/β, for stretched cells with various covering ratios (solid lines in Fig. S6*B*). For $\gamma < 2\beta$, the compact cell shapes discussed in *Two-dimensional ordered structure analysis,* $n_{\text{stretch}} = 1$ minimize the surface energy. For $\gamma > 2\beta$, surface cells that cover three bulk cells are always lower energy than cells which cover one, two, or four bulk cells, suggesting that the optimal covering ratio in 2D is three. Furthermore, Fig. S6*B* compares the surface tension calculated using the full cell shapes (solid lines) to the surface tension calculated for fixed bulk shapes (dashed lines). This figure illustrates that the simple, fixed bulk cell approximation is reasonable, and we will use it for the remainder of this section. A subset of these data is shown in the main text Fig. 5 *A* and *B*.

As illustrated in Fig. S6, this model predicts a quick crossover at $\gamma/\beta = 2$ from compact surface cell shapes to stretched surface cell shapes. Furthermore, the surface tension in units of β varies strongly with γ/β for $\gamma/\beta < 2$; adhesion is the dominant contribution to changes in surface tension. For $\gamma/\beta > 2$, the surface tension still increases with γ/β, but with a much smaller slope. In this regime, the contact area for surface cells begins to shrink as shown in Fig. S6*A*, and the dominant contributions are from β and the restoring force, α. Intuitively, for small values of γ/β, surface cells make fewer contacts than bulk cells, and therefore adhesive contacts are the dominant contribution to the surface tension. For large values of γ/β, cells stretch to make the same number of contacts, and so surface tension is controlled by other contributions to the energy such as cortical tension and adhesion regulation.

It is difficult to reconstruct all cell–cell interfaces accurately in an experiment, but the covering ratio is accessible experimentally. We can imagine taking 1D slices of a 2D aggregate at lines tangent to the surface of the aggregate, and calculating the projected length of each cell onto that line. The ratio of the projected length of surface cells to the projected length of bulk cells should be the same as this covering ratio, three. Three-dimensional ordered aggregates have two types of facets, denoted [001] and [011] in crystallographic notation, with different surface cell shapes along each facet. Using the same prism-spherical cap approximation as in *Three-dimensional cellular structures*, we find that [001] faces have a covering ratio of 2.16, and [011] faces have a covering ratio of 4.32. The covering ratio for the entire ordered aggregate depends on the relative sizes of these facets on the surface of the crystal, which is 27% type-[001] and 73% type-[011] (see Eq. **S18**). Therefore, we predict that the projected area of surface cells is 3.7 times greater than that of bulk cells.

Relationship Between Adhesion and Cortical Tension. As discussed in the main text, the effective adhesion in our model is understood to be the total energetic effect of contacting surfaces including local changes to the cortical network near the interface, instead of simply the adhesive bonds per se. Our model suggests that when surface cells are not stretched out, tissue surface tension scales with the "effective adhesion" γ, which involves the change in cortical tension $\Delta\beta$ at contacting interfaces, and the free energy per unit surface area for cadherin bonds Γ:

$$\gamma = \Gamma - 2\Delta\beta. \qquad \textbf{[S25]}$$

We call γ an effective adhesion because it is directly proportional to the contacting surface area between two cells.

Based on this equation, we can imagine two different scenarios: (*i*) $\Delta\beta < 0$ and (*ii*) $\Delta\beta > 0$. Because $\Delta\beta = \beta_C - \beta_{\text{NC}}$ is the difference between the cortical tension at contacting and noncontacting interfaces, one needs to determine if the cortical tension is enhanced or reduced near cell–cell contacts. There is experimental evidence that different scenarios may occur in different cell types. Because our mesoscopic model accommodates either case, it suggests some novel interpretations of existing experiments.

First, there are some observations that suggest $\Delta\beta < 0$, i.e., cortical tension is smaller at cell–cell contacts than at cell–culture medium interfaces. Recent experiments where retinal pigment epithelial cells are cultured on specific architectures suggest that the actin network is more dense in regions where the cells do not make adhesive contacts (S12, S13). Similarly, Yamada and Nelson (S14) have made detailed observations of cadherin dynamics in Madin–Darby canine kidney cells, and found that the cortical network is less dense at contacts, and a cortical-tension-increasing biochemical pathway is activated outside of the contact region.

Although it is unclear whether these epithelial cells form macroscopic three-dimensional aggregates with a measurable tissue surface tension, such an observation has very interesting implications. A major outstanding question in the field is how the tissue surface tensions, which are on the order of an erg/cm^2, can be generated by cadherin bonds which have a small binding

energy $10kT$, at least when the binding energy is measured by atomic force microscopy on short timescales (S15). In contrast, estimates for the cortical tension in tissues are much larger, on the order of an erg/cm^2. In tissues where $\Delta\beta$ is large and negative, Eq. **S25** explains how remodeling of the cortical network near contacts can account for the large measured tissue surface tension.

However, there are several tissue types where observations suggest $\Delta\beta > 0$. Phalloidin staining of zebrafish aggregate cells at high magnification suggests that the actin network is less dense at the cell-culture medium interface than at cell contacts (see Fig. S7). This result differs from the staining reported in ref. S16, but is in agreement with E-cadherin antibody staining which is also enriched at these sites, Fig. S7 *D* and *E*. Furthermore, cell–cell contacts between surface cells seem to have the highest E-cadherin accumulations (see Fig. S7), possibly because these are the sites of highest stress as these stretched cells are pulling on each other for force balance. Observations that the cortical tension increases near cell–cell contacts have been reported in S180 carcinoma cells by Chu et al. (S15).

If $\Delta\beta > 0$, then the free energy of mature cadherin bonds per unit area (Γ) must be much larger than the reported $\sim 10kT$. One possible explanation for this discrepancy is that mature cadherin bonds are additionally stabilized by alpha-catenin and actin on a timescale of about 10 min, and therefore mature bonds are much stronger than immature bonds. Another possibility is that there are additional bonds (such as integrin-mediated bonds) which are stronger and only form after the intial cadherin bonds are initiated.

In any case, our model suggests that cortical network remodeling near contact interfaces plays a large role in macroscopic tissue surface tension and therefore deserves more study. Both correlated and anticorrelated feedback between adhesion and cortical tension fit within the framework of our model.

Connection with Other Surface Tension Theories. Recent work by Brodland et al. (S17) addresses the microscopic origins of surface tension in terms of interfacial tensions, where γ_{cm} is the interfacial tension of a cell-medium interface and γ_{cc} is the interfacial tension of a cell–cell interface. Following Graner (S18), one can show that, if individual cells do not change their shapes, the surface tension should scale as

$$\sigma = \frac{\gamma_{cm} - \gamma_{cc}}{2}. \qquad \textbf{[S26]}$$

In our model, it is also possible for the interface between a cell and culture medium, which carries a tension $\gamma_{cm} = \beta$, to be different from cell–cell interfaces, which carry a tension $\gamma_{cc} = 2\beta - \gamma$. Inserting into Eq. **S26**, we find $\sigma = \gamma/2$, which is equivalent to the differential adhesion hypothesis and is represented by the dotted line in Fig. 2*A* in the main text.

However, experimental evidence indicates that the cells do change their shapes. Surface tension does not result solely from the line tensions—the surface tension depends on the geometry (or cell shapes) because it is an energy per unit area. In our model, the fact that a nonproliferating cell has a roughly constant volume constrains this geometry, and allows us to specify the surface tension exactly. Our analysis suggests that this shape change does not significantly alter the accuracy of the differential adhesion hypothesis when the adhesion and cortical tension are similar $0.186 < \gamma/\beta < 2$, but that geometric effects become important when the two are very different ($\gamma/\beta > 2$) and surface cells stretch.

1. Schoetz E-M, et al. (2008) Quantitative differences in tissue surface tension influence zebrafish germlayer positioning. *HFSP J* 2(1):1–56.
2. Schoetz E-M (2008) *Dynamics and Mechanics of Zebrafish Embryonic Tissues—A study of the physical properties of zebrafish germlayer cells and tissues and cell dynamics during early embryogenesis.* (Verlag Dr. Mueller Publishing Group, Saarbruecken).
3. Foty RA, Steinberg MS (2005) The differential adhesion hypothesis: A direct evaluation. *Dev Biol* 278:255–263.
4. Nose A, Nagafuchi A, Takeichi M. (1988) Expressed recombinant cadherins mediate cell sorting in model systems. *Cell* 54:993–1001.
5. Duguay D, Foty RA, Steinberg MS (2003) Cadherin-mediated cell adhesion and tissue segregation: Qualitative and quantitative determinants. *Dev Biol* 253:309-323.
6. Brakke KA (1992) The surface evolver. *Exp Math* 1(2):141–165.
7. Fortes MA, Rosa ME (2001) The surface energy and contact angles of a liquid foam. *J Colloid Interf Sci* 241:205–214.
8. Hufnagel L, Teleman AA, Rouault H, Cohen SM, Shraiman BI (2007) On the mechanism of wing size determination in fly development. *Proc Natl Acad Sci USA* 104:3835–3840.
9. Farhadifar R, Roper J-C, Aigouy B, Eaton S, Jlicher F (2007) The influence of cell mechanics, cell-cell interactions, and proliferation on epithelial packing. *Curr Biol* 17:2095–2104.
10. Weaire D, Phelan R (1994) A counter-example to Kelvin's conjecture on minimal surfaces. *Phil Mag Lett* 69:107–110.
11. Harrison O, et al. (2010) Two-step adhesive binding by classical cadherins. *Nat Struct Mol Biol* 3:348–357.
12. Thery M, Pepin A, Dressaire E, Chen Y, Bornens M (2006) Cell distribution of stress fibres in response to the geometry of the adhesive environment. *Cell Motil Cytoskel* 63:341–355.
13. Thery M, et al. (2006) Anisotropy of cell adhesive microenvironment governs cell internal organization and orientation of polarity. *Proc Natl Acad Sci USA* 103:19771–19776.
14. Yamada S, Nelson WJ (2007) Localized zones of Rho and Rac activities drive initiation and expansion of epithelial cell-cell adhesion. *J Cell Biol* 178:517–527.
15. Chu Y-S, et al. (2004) Force measurements in E-cadherin mediated cell doublets reveal rapid adhesion strengthened by actin cytoskeleton remodeling through Rac and Cdc42. *J Cell Biol* 167:1183–1194.
16. Krieg M, et al. (2008) Tensile forces govern germ-layer organization in zebrafish. *Nat Cell Biol* 10:429–436.
17. Brodland GW, Yang J, Sweny J (2009) Cellular interfacial and surface tensions determined from aggregate compression tests using a finite element model. *HFSP J* 4:273–281.
18. Graner F (1993) Can surface adhesion drive cell-rearrangement? Part I: Biological cell-sorting. *J Theor Biol* 164:455–476.

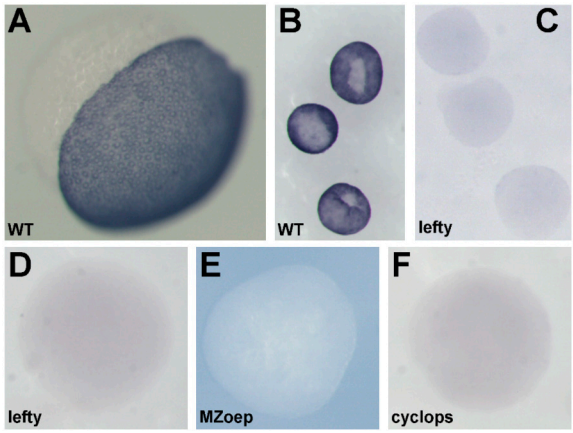

Fig. S1. Surface cells of zebrafish aggregates composed of ectoderm or mesendoderm cells do not express the enveloping layer (EVL) specific marker cyt-1. (*A*) Superficial cells (EVL) of wild-type embryos express *cyt-1* at shield stage. Cyt-1 expression is detectable as early as the late blastula stage (S7). (*B*) Aggregates from sphere stage wild-type embryos also show strong cyt-1 expression. In contrast, aggregates of wild-type embryos overexpressing Cyclops, lefty, or from maternal zygotic one-eyed pinhead (MZoep) mutants, representing mesendoderm or ectoderm tissues, respectively, do not express cyt-1 (*C–F*). These aggregates were shown previously (S1, S2) to homogenously express tissue type-specific markers for several hours in culture. This finding is in agreement with the results observed for deep cell explants in ref. S7.

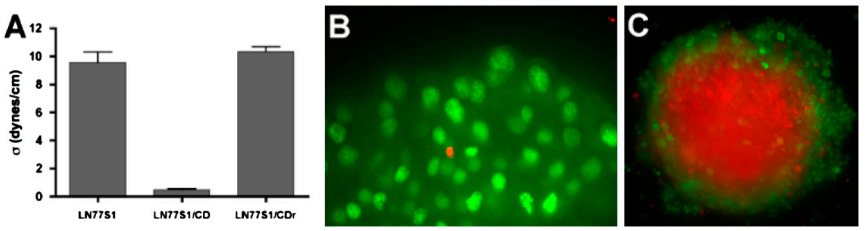

Fig. S2. (*A*) N-cadherin expressing L-cell aggregates recover from CD treatment. The cohesivity of aggregates of LN77S1 was markedly reduced upon treatment with CD. However, if aggregates were removed from CD and placed in fresh tissue culture medium, they recovered their cohesion to levels equaling, and sometimes surpassing, that of untreated aggregates. This result demonstrates that the effects of CD are reversible and suggests that CD treatment does not result in permanent cell damage. Similarly, injecting E- or N-cadherin morpholino does not appear to injure cells since a live/dead cell assay failed to identify the presence of any dead or dying cells in zebrafish ectoderm aggregates containing 6 ng E-cadherin MO (*B*), and injected N-cadherin MO treated mesendoderm (green) was able to sort out from mesendoderm (red) while in culture for over 25 h (*C*).

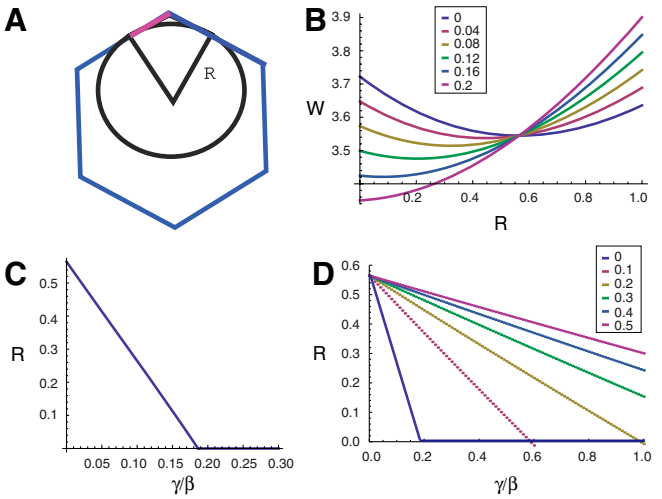

Fig. S3. Cavitation, or opening up of gaps between cells, in the mechanical model. (*A*) A diagram illustrating one corner of a hexagon with rounded corners. (*B*) A plot of the energy *W* as a function of the circle radius *R* for various values of the ratio between the adhesion and cortical tension (γ/β). (*C*) A plot of the minimum energy value of *R* as a function of the ratio γ/β. For $\gamma/\beta > 0.186$, $R^* = 0$ and the minimum energy packing is a hexagon with no rounded corners. (*D*) Plot of radii of curvature for cell corners as a function of γ/β. Different colors correspond to different values of the elasticity coefficient, α as indicated by the legend. As elasticity increases, the cells become rounded over a much larger parameter range in γ/β.

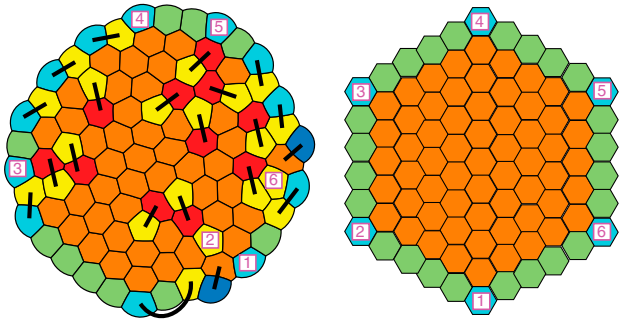

Fig. S4. (*A*) Illustration of a small cellular structure with finite boundary. Cells are colored according to their number of nearest neighbors, and cells are arbitrarily grouped into defect pairs using solid black lines. Magenta squares denote the remaining isolated disclinations. (*B*) Illustration of an ordered cellular structure with six isolated disclinations.

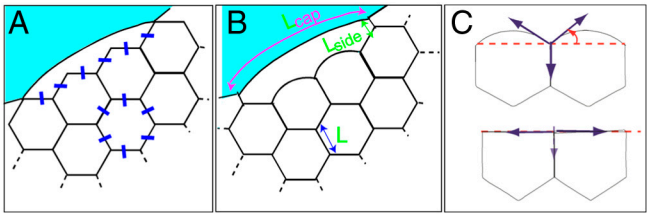

Fig. S5. Illustration of stretched surface cell shapes used in calculations. (*A*) Cells along the interface with the cell-culture medium can stretch to form the same number of contacts as in the bulk—for constant bulk cell shapes this means each surface cell covers approximately three interior cells. Compare to Fig. 1*C* in main text. (*B*) Cellular structures with stretched surface cells satisfy force balance and the constant area constraint when second-layer cells are curved. Stretched surface cells also contact one another over a fixed length L_{side}. These effects cancel one another so that the covering ratio calculated from *A* is approximately correct. (*C*) Illustration of line tensions at the surface of 2D aggregate. Aggregates where the interface between a cell and culture medium is rounded have a macroscopic surface tension that is different from the cortical tension. In contrast, if the cell-culture medium interface is flat then force balance requires that the macroscopic surface tension equal the cortical tension along that interface.

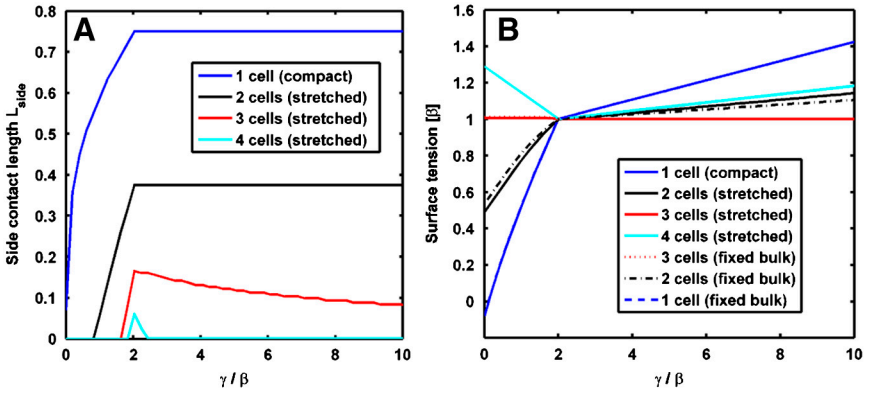

Fig. S6. (*A*) Contact length between surface cells L_{side} that minimizes the surface energy as a function of the ratio between the adhesion and cortical tension (γ/β). Each line corresponds to a different integer value for the covering ratio: The number of interior cells covered by the surface cell. (*B*) Surface tension as a function of γ/β for different values of the covering ratio. Solid lines correspond to calculations based on curved cell shapes that satisfy force balance. Dashed lines correspond to an approximation where the bulk cells maintain a fixed, hexagonal shape.

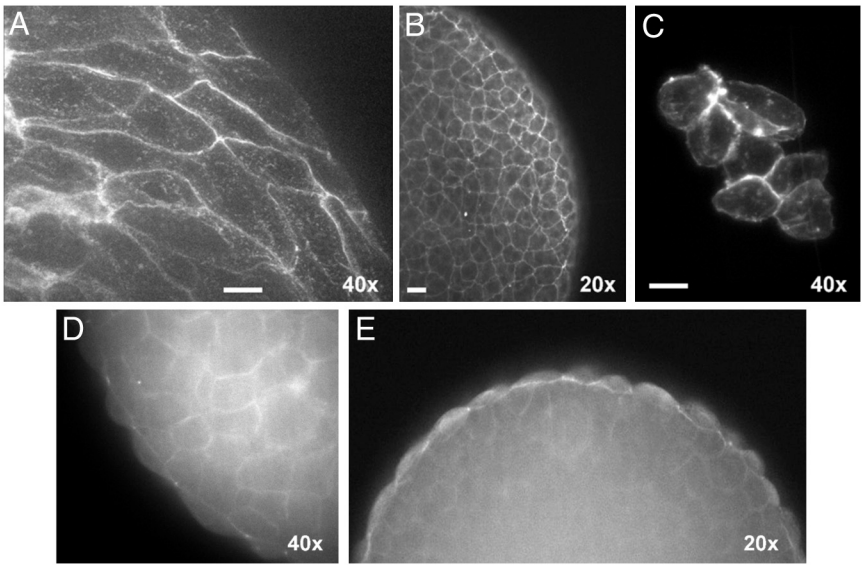

Fig. S7. (*A*) Maximum intensity projection of a part of a zebrafish ectoderm aggregate at 40× magnification. The cell membranes are labeled with Alexa546 phalloidin antibody which labels filamentous actin. Surface cells show punctate phalloidin staining at the interface with the cell-culture medium and stronger filamentous-like staining at cell–cell contacts. (*B*) Another ectoderm aggregate, but at 20× magnification to show a larger area. (*C*) A small cell cluster to focus in on the difference in staining between cell–cell interfaces and cell–medium interfaces. In all three images, the cell–cell interfaces have significantly stronger labeling than the cell–medium interfaces. (*D* and *E*) Equator confocal slice of a zebrafish ectoderm aggregate: E-cadherin antibody staining at 40× and 20×, respectively. The staining is strongest at cell–cell interfaces in correlation with phalloidin staining and in particular at contact points between neighboring surface cells (see also Movie S3).

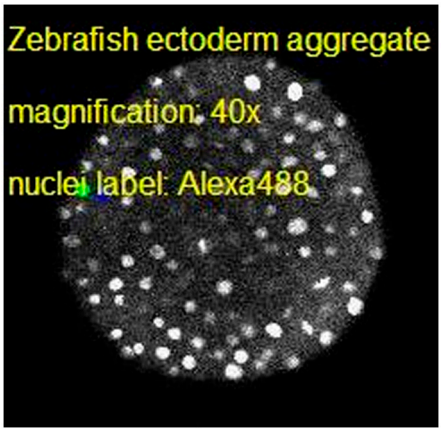

Movie S1. This movie shows a single *z* slice of a zebrafish ectoderm aggregate labeled with histone conjugated Alexa488. The cell nuclei are fluorescent. The movie was taken with a 40× objective on a two-photon microscope with 10-min time steps. Two cells are labeled artificially in blue and green to better illustrate their motion. Over the course of time, the blue cell moves outward toward the surface, while the green cell moves from the aggregate surface to the interior, illustrating the liquid character of the aggregate on long times. (Frame rate: 5 fps.)

Movie S1 (MOV)

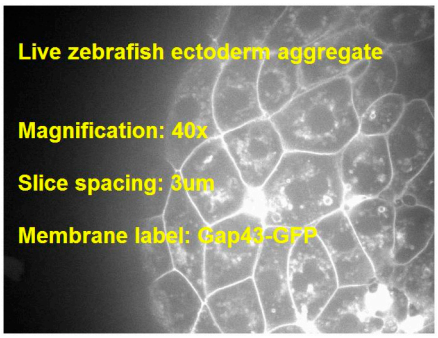

Movie S2. This movie shows a zebrafish ectoderm aggregate labeled with Gap43-GFP. The cell membranes are fluorescent. The movie was taken on an Olympus spinning disc confocal microscope at 40× magnification. Slices are 3 μm apart. The movie shows a *z* stack, starting from the outer surface of the aggregate toward the equatorial plane. The projected areas of the surface cells are much larger than of the bulk cells as quantified in the main part of this paper. (Frame rate: 5 fps.)

Movie S2 (MOV)

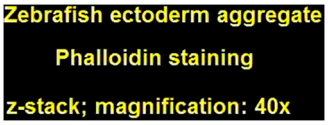

Movie S3. This movie shows a zebrafish ectoderm aggregate labeled with phalloidin FITC staining to visualize f-actin distribution. Actin distribution is punctate at the interfaces with the cell–culture medium and enforced at cell–cell interfaces. In particular, stretched surface cells show a strong actin accumulation at the contact areas with their neighbors, in agreement with the E-cadherin distribution shown in Fig. S7. The movie was taken on an Olympus spinning disc confocal microscope at 40× magnification and shows a *z* stack, starting from the outer surface of the aggregate toward the equatorial plane. (Frame rate: 5 fps.)

Movie S3 (MOV)

Table S1. Surface Evolver data showing that the projected lengths of defect pairs at the surface change significantly for low γ/β, but their energies remain relatively constant

γ/β	σ	$\%\Delta l_{proj}$	$\%\Delta W_{surf}$	$\%\Delta W_{int}$
0.33	0.147 ± 0.004	−9.2 ± 3.3	−0.2 ± 0.2	0.1 ± 0.2
0.75	0.414 ± 0.006	−8.4 ± 3.6	−0.4 ± 0.6	0.1 ± 0.2
1.0	0.553 ± 0.006	−7.9 ± 3.7	−0.7 ± 0.9	0.1 ± 0.2
1.5	0.795 ± 0.005	−7.6 ± 2.9	−2.4 ± 1.4	0.1 ± 0.2
1.66	0.868 ± 0.004	−7.7 ± 2.8	−3.6 ± 1.6	0.1 ± 0.2